Journal of Quantitative Spectroscopy & Radiative Transfer 163 (2015) 120–141

Contents lists available at ScienceDirect

Journal of Quantitative Spectroscopy & Radiative Transfer

journal homepage: www.elsevier.com/locate/jqsrt

Temperature dependences of N_2-broadening and shift coefficients in the ν_6 perpendicular band of $^{12}CH_3D$

A. Predoi-Cross [a,*], V. Malathy Devi [b], K. Sung [c], T. Sinyakova [d], J. Buldyreva [d], D. Chris Benner [b], M.A.H. Smith [e], A.W. Mantz [f]

[a] Department of Physics and Astronomy, University of Lethbridge, Lethbridge, AB, Canada T1K 6R4
[b] Department of Physics, The College of William and Mary, Williamsburg, VA 23187, USA
[c] Jet Propulsion Laboratory, California Institute of Technology, Pasadena, CA 91109, USA
[d] Institute UTINAM UMR CNRS 6213, University of Franche-Comte, 25030 Besancon, France
[e] Science Directorate, NASA Langley Research Center, Hampton, VA 23681, USA
[f] Department of Physics, Astronomy and Geophysics, Connecticut College, New London, CT 06320, USA

ARTICLE INFO

Article history:
Received 19 March 2015
Received in revised form
11 May 2015
Accepted 12 May 2015
Available online 22 May 2015

Keywords:
Monodeuterated methane
Infrared spectra
Nitrogen-broadening
Temperature dependences of widths and shifts
Line mixing
Spectral line shapes

ABSTRACT

The temperature-dependences of line broadening and shift parameters for many $^{12}CH_3D$ transitions have been determined using six high-resolution, high signal-to-noise ratio, room-temperature CH_3D (98% purity) and CH_3D-N_2 spectra recorded with 25 cm path length (at 0.01 cm^{-1} unapodized resolution) using the McMath–Pierce FTS located on Kitt Peak, Arizona, and 17 additional high quality, pure CH_3D (99% purity) and CH_3D-N_2 spectra recorded between 79 and 296 K with the 20.38 cm path coolable cell (at 0.0056 cm^{-1} unapodized resolution) with the Bruker 125HR FTS at the Jet Propulsion Laboratory (JPL), Pasadena, California. The spectra have been fitted simultaneously applying a multispectrum nonlinear least-squares technique. In the analysis, the Lorentzian N_2-broadened half-width coefficients and the corresponding pressure-shift coefficients as well as their temperature dependences are extracted for about 400 transitions ($0 \le J'' \le 19$, $K'' \le 16$) in the perpendicular ($\Delta K = \pm 1$) ν_6 band. At 296 K, the measured N_2-broadened half-width coefficients range from 0.0209 to 0.0782 cm^{-1} atm^{-1} whereas the majority of the associated N_2-induced shift coefficients are negative, and the values are between -0.016 and 0.005 cm^{-1} atm^{-1}. The temperature dependence exponents for N_2-broadened half-widths range between 0.264 and 0.924, whereas the temperature dependence coefficients for N_2-induced shifts are between 0 and 0.00011 cm^{-1} atm^{-1} K^{-1}. The N_2-broadened half-width coefficients have been also calculated using a semi-classical approach based on a rigorous treatment of the active molecule as a symmetric top, a model intermolecular potential comprising both short- and long-range interactions, and exact classical trajectories. The role of the various high-order multipoles in the line-broadening at low, middle and high values of the rotational quantum number J'' has been investigated and the main features of the K-dependences analyzed. The calculations performed for 296, 240 and 190 K have allowed to deduce the half-width temperature-dependence exponents, completing the general comparison of our new experimental results with those which are available in the literature.

© 2015 Elsevier Ltd. All rights reserved.

* Corresponding author. Tel.: +1 403 329 2697; fax: +1 403 329 2057.
E-mail address: adriana.predoicross@uleth.ca (A. Predoi-Cross).

http://dx.doi.org/10.1016/j.jqsrt.2015.05.006
0022-4073/© 2015 Elsevier Ltd. All rights reserved.

1. Introduction

Methane is a prominent atmospheric trace gas and the third most abundant greenhouse gas in many regions of the world [1,2]. The sources of methane are both natural, such as wetlands and methane-outgassing from oceans [3], and anthropogenic, such as animal husbandry and fossil-fuel extraction [4]. The methane sinks include processes in atmospheric chemistry such as reactions with hydroxyl radicals [5] and natural processes in soil [6].

Besides the main isotopologue CH_4, the monodeuterated species CH_3D is highly important for understanding various atmospheric processes. In the Earth's atmosphere, stratospheric profiles of CH_3D mixing ratios have been retrieved using high-resolution solar occultation infrared spectra from the Atmospheric Trace MOlecule Spectroscopy (ATMOS) satellite instrument [7,8] and references therein. CH_3D is also an isotopic tracer present (or expected to be present) in many planetary atmospheres such as those of Jupiter, Saturn [9–11], Uranus [12–14], Mars [15–18], Titan [19–23], and subject to transport and chemical effects. It has also been identified in cometary spectra [24,25]. The concentrations of CH_3D and those of the parent molecule CH_4 are used to calculate the D/H ratios in these celestial bodies [26].

The atmosphere of Titan contains about 5% of methane and mostly nitrogen. The Composite InfraRed Spectrometer (CIRS) instrument on the Cassini spacecraft is monitoring Titan's thermal emission spectrum through three focal planes, one of them covering the spectral range of the CH_3D ν_6 band [23]. Knowledge of the temperature-dependence of N_2-broadened line widths and shifts over the Titan atmospheric temperature range (70 – 200 K) is needed for correct interpretation of IR spectra of Titan's atmosphere, such as those obtained by the CIRS instrument (for example, [23]). Bands of the three most abundant methane isotopologues ($^{12}CH_4$, $^{13}CH_4$ and CH_3D) in the spectral region from 6 to 10 microns are used not only for detection of atmospheric composition, but also for retrievals of Titan atmospheric temperature profiles and determination of $^{13}C/^{12}C$ and D/H ratios [23,26].

Most of the measured methane line widths happen to increase as a power law when temperature is decreasing. There have been several spectroscopic studies related to the spectral line shapes (e.g., Lorentz widths, pressure-shifts) of the ν_6 band of CH_3D [27–35]. N_2-broadened widths and N_2-induced shifts of $^{12}CH_3D$ lines have been measured at room temperature for transitions in the ν_2 [36], ν_3 [37–39], ν_5 [40], ν_6 [35], and $2\nu_4$ [41] bands. For low temperatures, measurements of only 10 N_2-broadened line-width coefficients of individual CH_3D lines in the ν_2 [42], ν_3 and ν_6 [43] bands are available in the literature, and spectroscopic databases (e.g., HITRAN [44]) currently list only a constant default value for the temperature dependences of the CH_3D line widths. Reports of selected room-temperature line mixing via off-diagonal relaxation matrix element coefficients for transitions of CH_3D broadened by N_2 in the ν_3 [39], ν_5 [40], and ν_6 [35] bands.

In 2002 [35] we reported Lorentz self- and nitrogen-broadened line-width coefficients as well as corresponding line-shift coefficients for more than 480 transitions in six sub-branches (^{P}P, ^{P}Q, ^{P}R, ^{R}P, ^{R}Q, ^{R}R) of the ν_6 (E) perpendicular band of $^{12}CH_3D$. These results were obtained from multispectrum fits of 14 – 17 spectra recorded at room temperature in the 1035-1270 cm^{-1} spectral range using two different Fourier-transform spectrometers, namely the McMath – Pierce FTS formerly located on Kitt Peak, Arizona, and the Bruker IFS 120 HR FTS located at the Pacific Northwest National Laboratory, Richland, Washington. The spectra were recorded using absorption path lengths of 10, 19.95, 25, 150, and 2486 cm, respectively. The gas total pressures ranged from 0.11 to 303 Torr for pure CH_3D and from 103 to 403 Torr for lean mixtures (~0.01 volume mixing ratios) of CH_3D and nitrogen.

To retrieve the temperature dependences of line-shape parameters, 17 new spectra of both pure (99%) CH_3D and dilute mixtures (0.003 – 0.0164 volume mixing ratios) of the same high-purity CH_3D sample in research grade nitrogen have been recorded from room to low temperatures using the coolable absorption cell with a path length of 20.38 cm (see [45] for its detailed description). The simultaneous multispectrum analysis [46] of the 17 new spectra and the six previous spectra [35] has allowed the determination of N_2-broadened line-width and N_2-pressure-induced line-shift coefficients and their temperature dependences for a large number of transitions. In addition, N_2- line mixing coefficients for 17 pairs of transitions via the off-diagonal relaxation matrix element formalism [46,47] have been also obtained.

However, unlike the line-width and pressure-shift coefficients, the temperature dependences of the relaxation matrix element coefficients could not be determined reliably for all measured mixed pairs. In such instances, a default value of 0.75 has been applied for other line-mixed pairs in the least squares fittings.

2. Experimental details and data analysis

As mentioned above, six of the 23 infrared absorption spectra analyzed in this study were from the set of room-temperature spectra previously used to study N_2- and self-broadening in $^{12}CH_3D$ transitions in the Triad region [35,36,40]. These spectra were recorded using the Kitt Peak FTS with an unapodized resolution of 0.01 cm^{-1} and signal-to-noise (S/N) ratios of about 700 and covered the spectral region 690 – 2840 cm^{-1}. Two of the six spectra recorded at low-pressure (1 – 3 Torr) and high-purity (98% enriched CH_3D from ICON isotopes) were important in the present study to determine the "zero-pressure" line centers of the $^{12}CH_3D$ transitions.

A set of 17 new high-resolution (0.0056 cm^{-1}), high S/N (> 1000) spectra were recorded in 2010 covering the 1070 – 1540 cm^{-1} spectral region, using the Bruker IFS 125HR Fourier transform spectrometer at the Jet Propulsion Laboratory. For recording these new spectra a specially designed and built 20.38 cm straight-path coolable absorption cell [45] was used. Various CH_3D and CH_3D+N_2 gas pressures, temperatures and volume mixing ratios of CH_3D were used to obtain these experimental spectra. A few low-pressure pure CH_3D spectra were acquired with the Bruker FTS as well, in order to more accurately

Table 1
Details on the experimental setup and physical conditions of spectra.

Configuration and conditions	JPL FTS Bruker 125 HR	McMath-Pierce Kitt Peak FTS
Useable band pass (cm^{-1})	1000–1540	1050–2400
Light source	Globar	Globar
Beam splitter	KBr	KCl
Detector	HgCdTe	He cooled As:Si
Resolution (cm^{-1}) (unapodized)	0.0056	0.01
Maximum optical path difference (cm)	90.00	49.99
Aperture diameter (mm)	1.5	8
Sample pressure (Torr)	See Table 2	See Table 2
Temperature[c] (K)	79 – 296 K	296.0 – 296.6 K
Cell path length (cm)	20.38	25 cm
Cell windows (wedged)	KBr	KCl
Scanning time (hours)	~2	1.1 (10 coadds)
Signal-to-noise	~1100–1800	~700
Calibration standards	ν_2 lines H_2O [48]	ν_2 lines H_2O [48]

Table 2
Summary of the experimental conditions of the CH_3D spectra.

Temperature (K)	Gas mixture	CH_3D VMR	Path (cm)	Pressure (Torr)	Calibration correction [a]	RMS[b]
296.60	CH_3D	1.0	25.0	1.013	0.9999998059	0.115
295.45	CH_3D	1.0	25.0	3.050	0.9999998708	0.113
296.20	CH_3D+N_2	0.0133	25.0	102.50	0.9999997940	0.105
296.40	CH_3D+N_2	0.0133	25.0	202.10	0.9999998054	0.099
296.40	CH_3D+N_2	0.0133	25.0	302.55	0.9999998144	0.104
296.40	CH_3D+N_2	0.0136	25.0	402.25	0.9999998200	0.112
296.00	CH_3D+N_2	0.00362	20.38	250.60	1.0000002644	0.088
296.00	CH_3D+N_2	0.00365	20.38	728.94	1.0000002853	0.093
239.65	CH_3D+N_2	0.00983	20.38	194.99	1.0000002702	0.091
240.15	CH_3D+N_2	0.01575	20.38	444.04	1.0000002712	0.110
239.65	CH_3D+N_2	0.00990	20.38	602.23	1.0000002710	0.098
189.65	CH_3D	1.0	20.38	7.10	1.0000002625	0.100
188.65	CH_3D+N_2	0.01302	20.38	152.72	1.0000002738	0.088
188.65	CH_3D+N_2	0.0037	20.38	256.82	1.0000002616	0.079
189.15	CH_3D+N_2	0.0133	20.38	546.30	1.0000002669	0.096
135.15	CH_3D	1.0	20.38	2.58	1.0000002747	
133.35	CH_3D+N_2	0.00512	20.38	177.67	1.0000002771	0.085
133.35	CH_3D+N_2	0.01635	20.38	246.38	1.0000002758	
133.35	CH_3D+N_2	0.00515	20.38	503.86	1.0000002739	0.085
78.75	CH_3D	1.0	20.38	8.5	1.0000002744	
77.65	CH_3D+N_2	0.0127	20.38	100.90	1.0000002796	0.094
75.15	CH_3D+N_2	0.00339	20.38	295.28	1.0000002774	0.092
76.95	CH_3D+N_2	0.0119	20.38	642.12	1.0000002788	

Note: 760 Torr = 1 atm = 101.325 kPa.
[a] Wavenumber scales were calibrated relative to ν_2 water vapor line positions by Toth [48].
[b] The RMS values correspond to the multispectrum fit residuals plotted in Fig. 3(b).

determine the zero-pressure line positions (since these spectra had higher resolution than the low-pressure Kitt Peak spectra).

All 23 spectra were simultaneously fitted using a multispectrum nonlinear least-squares technique [46]. Details on the experimental setups for the two sets of measurements are provided in Table 1. The experimental physical conditions of the spectra analyzed are presented in Table 2. Transitions belonging to all bands in the Triad (ν_3, ν_6 and ν_5) were observed in both sets of spectra. Spectroscopic results pertaining to only the ν_6 perpendicular band of $^{12}CH_3D$ will be presented in this article. Results for the parallel band ν_3 and the perpendicular band ν_5 will be reported in a subsequent article.

3. Retrievals of line parameters

Prior to the multispectrum fittings the wavenumber scales of both datasets were calibrated using reference water vapor line positions [48]. In the case of Kitt Peak data, these water vapor lines had two components, a narrow line due to residual gas in the evacuated FTS chamber as well as a broad feature from atmospheric-pressure optical paths outside the FTS and sample cell purged with dry nitrogen vapor to minimize H_2O absorptions interfering with the CH_3D transitions. In the JPL Bruker spectra, the water lines arose only from small amounts of residual gas in the evacuated FTS chamber. The wavenumber calibration factors determined for each

of the fitted spectra are included in Table 2. In both sets of experiments, the sample pressures and temperatures were continually monitored during the measurements using appropriate calibrated pressure gauges and temperature sensors [35,45].

The spectral line parameters in the HITRAN2008 database [49] were used as initial guesses for starting the multispectrum fittings. Before starting the fits, it was also necessary to establish the isotopologue abundances (e.g., $^{12}CH_4$, $^{13}CH_4$, $^{12}CH_3D$ and $^{13}CH_3D$) in the CH_3D samples. Initial estimates of the isotopologue abundances were made based upon the % D-enrichments stated by the manufacturer (ICON Isotopes). Small adjustments to these isotopologue abundances were needed when the spectra were fit simultaneously. These values were established by fitting several selected regions of each spectrum prior to analyzing all of the fitted regions. Once the isotopologue abundances were determined, they remained the same for the corresponding spectra in all fitted regions.

Low-pressure pure CH_3D spectra at room temperature were fitted first and N_2-broadened spectra at room temperature were then added, one spectrum at a time, until all room-temperature spectra were fitted simultaneously. This process allowed the initial determination of room temperature N_2-broadened width and shift coefficients for the strong, unblended lines. Subsequently, low temperature pure CH_3D and N_2-broadened CH_3D spectra were added one spectrum at a time, as appropriate. The volume mixing ratios of N_2-broadened spectra were carefully adjusted (when appropriate) while the temperature dependences of Lorentz self- and N_2-broadened width and shift coefficients of various lines were adjusted until all the spectra were fit satisfactorily such that the weighted (observed minus calculated) fit residuals from all fitted spectra were minimized and no noticeable features were observed in the residuals.

N_2- and self-broadened line-width, pressure-shift and the relaxation matrix element coefficients (where appropriate) were retrieved using the multispectrum fitting procedure that has been described in several of our prior studies (for example: [34–36,39–40,46–47]). Spectral intervals of $5-15\ \mathrm{cm}^{-1}$ wide from each of the 23 spectra were fitted simultaneously. The total number of spectra fitted in each interval varied between 19 and 23, depending upon whether $^{12}CH_3D$ features were apparent at the volume mixing ratios and gas sample pressures of the chosen spectra. For strong CH_3D transitions the line positions, intensities, N_2-broadening coefficients and their temperature dependence exponents, N_2-induced shift coefficients and their temperature dependence coefficients were adjusted until the sum of the squares of the weighted fit residuals between the observed and calculated line profiles were minimized.

Line mixing (off-diagonal relaxation matrix element, or ORME) coefficients between selected pairs of transitions were also determined, where possible. Even though the temperatures of the gas samples ranged between 296 K and 75 K, in several cases, it was not possible to measure with confidence the temperature dependences of the relaxation element coefficients. An improved theoretical model for the temperature-dependence of CH_3D line mixing is needed to measure these parameters correctly and reliably. Where their values were not determined, the temperature dependence exponents were fixed to a default value of 0.75, similar to the default value applied for the temperature dependence exponents of the line-width coefficients..

Although several (see Table 2) pure CH_3D spectra were included in the analysis, the pressures were not high enough to retrieve reliable information on self-broadening and self-shift coefficients for all observed transitions. The pure CH_3D gas pressures were in an intermediate range so that we could not completely ignore their values. This means that in some instances (e.g., low-temperature spectra) it was necessary to adjust the self-broadening and its temperature dependence exponent to obtain a best fit. However, while many self-broadening coefficients and their temperature dependences could be determined from our spectra, it was not possible to measure any reliable self- pressure-shift coefficients or their temperature dependence coefficients.

As in previous studies using the multispectrum fitting technique, the Lorentz N_2-broadened line-width coefficients, N_2-induced line-shift coefficients and their temperature dependences were measured on a line-by-line basis using the following equations:

$$b_L(p,T) = p\left[b_L^0(N_2)(p_0,T_0)(1-\chi)\left[\frac{T_0}{T}\right]^{n1} + b_L^0(\mathrm{self})(p_0,T_0)\chi\left[\frac{T_0}{T}\right]^{n2}\right] \quad (1)$$

$$\nu = \nu_0 + p\left[\delta^0(N_2)(1-\chi) + \delta^0(\mathrm{self})\chi\right] \quad (2)$$

$$\delta^0(T) = \delta^0(T_0) + \delta'(T-T_0) \quad (3)$$

where b_L^0 and δ^0 represent pressure broadening and pressure-shift coefficients (in $\mathrm{cm}^{-1}\ \mathrm{atm}^{-1}$ at T_0=296 K), respectively. $b_L(p,T)$ is the Lorentz half-width (in cm^{-1}) of the spectral line at pressure p and temperature T, b_L^0 (*Gas*) (p_0,T_0) is the Lorentz half-width coefficient of the line at the reference pressure p_0 (1 atm) and temperature T_0 of the broadening gas (either N_2 or CH_3D). χ is the ratio of the partial pressure of CH_3D to the total gas pressure in the cell. The temperature dependence coefficients of the Lorentz half-width coefficient are n_1 (for N_2) and n_2 (for CH_3D). The temperature dependence of the N_2-pressure-shift coefficients is $\delta'(N_2)$. Temperature dependences of N_2- and self-broadened (in a few cases) half-width and pressure-induced shift coefficients were measured separately for each transition within the same fit. As shown in Eq. (3) a linear law was used for to model the temperature dependences of pressure-induced shift coefficients.

Self- and N_2-broadened widths and the temperature dependence exponents for the broadening coefficients for all transitions were initially fixed to values in the HITRAN2008 database [49] and depend upon the rotational quantum numbers of the transition. Indeed, in the HITRAN databases ([44,49]) only the self- and air-broadened line-width coefficients are listed and we have assumed that the N_2-width coefficients for the unmeasured transitions are the same as the air-broadened width coefficients. For parameters not

included in HITRAN [44,49], the initial values for all transitions were set at reasonable default values estimated from our previous studies of CH_3D [35], $^{12}CH_4$ and $^{13}CH_4$ [50–53] in the thermal infrared. The pressure-broadened self- and N_2-width, self- and N_2-shift coefficients and their temperature dependence values were 0.085 cm^{-1} atm^{-1}, 0.065 cm^{-1} atm^{-1}, -0.003 cm^{-1} atm^{-1}, −0.002 cm^{-1} atm^{-1}, 0.75 and 0.75, respectively. The temperature-dependence coefficients for self- and N_2-induced shift for all lines were initially set to default values of 0.00002 cm^{-1} atm^{-1} K^{-1} instead of zero, based upon our previous studies of self- and air-broadening in $^{12}CH_4$ and $^{13}CH_4$ [50–53] in the same spectral region. For unmeasured lines the parameters remained fixed to these default values. This assumption introduced no noticeable residuals in the least squares fits (see Figs. 3 and 4).

For weaker transitions for which broadening and shift coefficients could not be determined, only their line positions and intensities were adjusted in the multispectrum fits. Several weak unidentified features (trace contaminants of unknown origin or $^{13}CH_3D$ transitions) appeared in some of the fitted regions and were included as unidentified transitions in the fit. The broadening and shift parameters of these unidentified features remained fixed to the default values described above.

During the analysis, it was noticed that, in order to minimize the fit residuals, the gas sample temperatures, especially for the lowest temperature (~79 K) dataset, apparently needed adjustments in the range -0.5 to -4.2 K from the ones given by the temperature sensors during the experiments. These adjustments were required in order to fit all of the spectra using the power-law expression (Eq. (1)) for temperature dependence of the line-widths, and the adjusted temperatures may not necessarily represent the actual physical temperatures of the gas samples. Departures from the power law have been evidenced by others and this confirms that such a law is approximate and that efforts in the theory are needed to derive more elaborate dependences.

At this time, we would like to attribute this need for temperature adjustments to be related to the small departures from the power-law temperature dependence of the Lorentz line-width coefficients that were observed over the same temperature range with the fit of the $^{13}CH_4$ R(2) manifold (See Ref. [45] and references cited therein). With this temperature adjustment we were still able to use Eq. (1) to obtain best-fit residuals in all our fitted intervals (e.g., Figs. 3 and 4). In the present analysis we have not made further efforts to fully characterize this temperature behavior of the Lorentz width coefficients, and our measured line-width coefficients could be characterized as the "effective line-width coefficients" with their temperature dependence exponents still enforced by Eq. (1). The actual temperature values used in the fits are listed in Table 2 rather than the measured temperatures so that the resulting effective line-width parameters can be compared with future experimental studies.

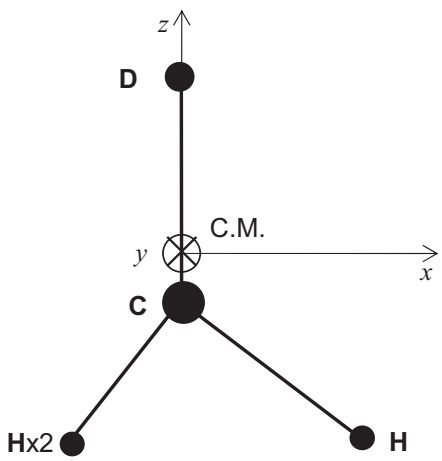

Fig. 1. Molecular frame and geometry parameters for the CH_3D molecule: |CH|=|CD|=1.08601 Å [60], ∠DCH=109.46667°.

4. Theoretical modeling of N_2-broadening coefficients and their temperature dependences for CH_3D transitions

Theoretical estimations of pressure-broadened CH_3D line widths were performed solely for the case of perturbation by nitrogen. Indeed, for this active molecule with a very small electric dipole moment (0.057 D [54]) and a vanishing quadrupole moment, the long-range interactions with an identical partner are very weak whereas the short-range interactions (typically modeled by pairwise atom-atom Lennard–Jones potentials) are determined by atom-atom parameters whose values are available in the literature. We note that the parameter values from different sources are sometimes inconsistent. For collisions with nitrogen, the intermolecular potential is expected to be modeled in a more reliable manner because of stronger electrostatic interactions.

Table 4
Atomic distances to the molecular centers of mass (calculated with the geometry of Fig. 1 for CH_3D and taken from [61] (for N_2) and atom-atom Lennard–Jones parameters [65] (for CH_3D-N_2 interactions).

r_{1i}, r_{2j} (Å)	d_{ij} (10^{-7} erg Å^{12})	e_{ij} (10^{-10} erg Å^6)
r_{1C}=0.0641	d_{CN}=0.3234	e_{CN}=0.2922
r_{1D}=1.0219	d_{HN}=0.0571	e_{HN}=0.0803
r_{1H}=1.1090	d_{DN}=0.0571	e_{DN}=0.0803
r_{2N}=0.550		

Table 3
Molecular parameters for CH_3D and N_2 used in the calculations: dipole moments μ, quadrupole moments Q, octopole moments Ω, mean polarizabilities α, polarizability anisotropies γ and hyper-polarizabilities $A_{||}$ and $A_{\perp}$ (α, γ, $A_{||}$and $A_{\perp}$ for CH_3D are those of CH_4).

Molecule	μ (D)	Q (D Å)	Ω (D Å^2)	α (Å^3)	γ	$A_{||}$=$A_{\perp}$ (Å^4)
CH_3D	0.057 [54]	0	3.10 [62]	2.59 [63]	0	0.82 [37]
N_2	0	−1.3 [61]	0	1.74 [63]	0.137 [64]	0

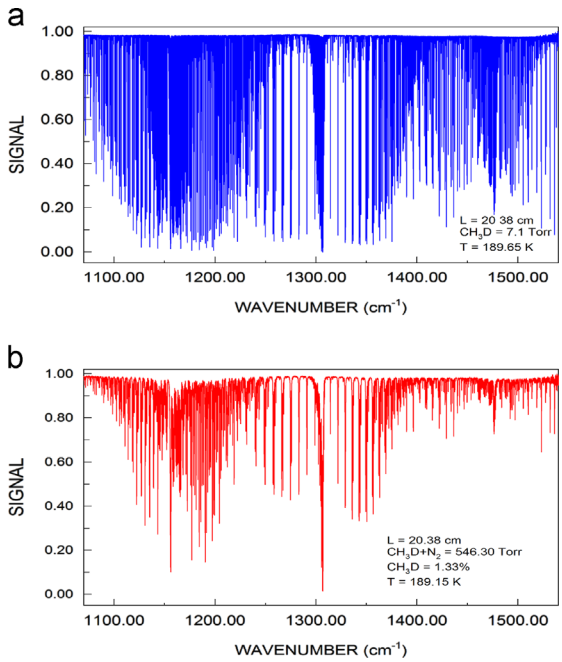

Fig. 2. Two laboratory absorption spectra of $^{12}CH_3D$ in the Triad region between 1070 and 1540 cm^{-1} recorded at 0.0056 cm^{-1} resolution with the Bruker FTS at JPL. The spectrum shown in the top panel (a) corresponds to 99% pure $^{12}CH_3D$ sample and the one shown in the bottom panel (b) is a dilute mixture of the 99% high-purity $^{12}CH_3D$ sample in nitrogen. Both spectra were taken near 189 K and using the 20.38 cm coolable cell (see text for details).

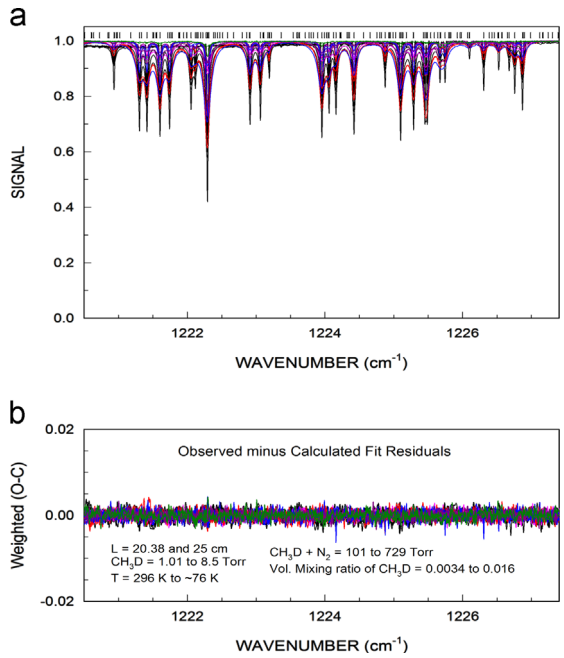

Fig. 3. A sample fitted interval in the $^{12}CH_3D$ Triad. Transitions belonging to both the ν_3 and ν_6 bands appear in this region. The experimental spectra are plotted in the upper panel (a) and the weighted observed minus calculated differences are shown in the lower panel (b). 20 of the possible 23 spectra are included in the fit. Small residuals (< 1% deep) still persist in one of the spectra that could not completely be fitted out. Some of these could belong to $^{13}CH_3D$ transitions for which assignments were not available when the present analysis was performed. Color codes: room-temperature spectra with the 25 cm cell (black), room-temperature spectra with the 20.38 cm cell (pink); spectra at 240 K (red); spectra at 189 K (blue); spectra at ~135 K (dark pink); spectra at ~76 K (dark green). (For interpretation of the references to color in this figure legend, the reader is referred to the web version of this article.)

Calculations of N_2-broadened line widths in the ν_6 band of CH_3D were performed with the standard expression of the semi-classical formalism of Robert and Bonamy [55]:

$$\gamma_{if} = \frac{n_2 \overline{v}}{2\pi c} \int_0^{\infty} 2\pi b db \langle 1 - e^{-\mathrm{Re}\, S_2} \rangle_{J_2} \tag{4}$$

where γ_{if} (in cm^{-1}) is the half-width of the line corresponding to the radiative transition $i \rightarrow f$. n_2 is the number density of the perturbing molecules; $\overline{v} = \sqrt{8kT/\pi m^*}$ is the mean relative thermal velocity (k is the Boltzmann constant, T is the temperature in Kelvin and m^* is the reduced mass of the molecular pair). The real part of the second-order contribution to the scattering matrix S_2 is averaged over the J_2 rotational states of the perturbing gas and integrated over the impact parameter b. We notice that the modified formula suggested by Ma et al. [56] and performing the average over J_2 states as the cumulated average (inside the exponential function) leads to overestimated values, so that we preferred not to employ it for our calculations.

The integration over trajectories required for computations of various S_2 terms was made with the exact-trajectory model [57–59] and the rotationally invariant representation of the interaction potential between the active (indexed by 1) and the perturbing (indexed by 2) molecules:

$$V(1,2,\vec{r}) = \sum_{l_1 l_2 l k_1} V^{k_1}_{l_1 l_2 l}(r) \sum_{m_1 m_2 m} C^{lm}_{l_1 m_1\ l_2 m_2} D^{l_1}_{m_1\ k_1}{}^{*} \times (\varphi_1, \theta_1, \chi_1) D^{l_2}_{m_2\ 0}{}^{*}(\varphi_2, \theta_2, \chi_2) C^{*}_{lm}(\theta, \varphi) \tag{5}$$

In this equation the products of rotational Wigner matrices and the spherical harmonics C^{lm} (normalized to $\sqrt{4\pi/(2l+1)}$) $D^{l_1}_{m_1\ k_1}{}^{*}(\varphi_1, \theta_1, \chi_1) D^{l_2}_{m_2\ 0}{}^{*}(\varphi_2, \theta_2, \chi_2) C^{*}_{lm}(\theta, \varphi)$ represent the rotationally invariant basis in the laboratory fixed frame (asterisks mark the complex conjugation), $C^{lm}_{l_1 m_1 l_2 m_2}$ are the Clebsch – Gordan coefficients. The radial potential components $V^{k_1}_{l_1 l_2 l}(r)$ contain contributions from various kinds of intermolecular interactions. We expressed the potential as a sum of electrostatic (e), induction (i) and dispersion (d) long-range terms completed by pairwise atom – atom (a) terms accounting for the short-range forces (the explicit forms of radial potential components and second-order contributions to the scattering matrix can be found in [59]).

Contrary to a previous simplified semi-classical calculation for the ν_2 parallel band [36] in which the three hydrogen atoms were projected on the principal molecular symmetry axis to form a linear molecule with CH_3D, we kept the real geometry of the equilibrium configuration (see Fig. 1), i.e. accurately treating the active molecule as a symmetric top. Because of the important role of the atom-atom terms in the quite weakly interacting CH_3D-N_2 system this more realistic configuration of hydrogen atoms is expected to ensure a better description of intermolecular interactions and more reliable line width values. After

Table 5
Experimental and calculated N_2-broadened line parameters and experimental self-broadened line parameters [see Eqs. (1–3) for the notations] in the ν_6 band of CH_3D. S are the symmetry labels and the ′ and ″ refer to the upper and lower states corresponding to each transition.

Position, cm^{-1}	J′	K′	S′	J″	K″	S″	Assignment	Int*10^{25}[a]	$b_L^0(N_2)$ expt,[b]	$b_L^0(N_2)$ calc.[b]	n_1 expt	n_1 calc.	$\delta^0(N_2)$ expt[b]	$\delta'(N_2)$ expt[c]	$b_L^0(self)$ expt[b]	n_2 expt
1080.746222(15)	10	3	E	11	4	E	^{P}P(11,4,E)	8.75(2)	0.0569(3)	0.0562	0.750(24)	0.630(1)				
1080.941134(7)	8	1	A1	9	0	A2	^{R}P(9,0,A2)	18.98(2)	0.0635(2)	0.0608	0.811(7)	0.678(4)	−0.00251(16)		0.0836(9)	0.798(14)
1082.344848(29)	7	4	A2	8	3	A1	^{R}P(8,3,A1)	5.34(1)	0.0620(2)	0.0597	0.802(5)	0.665(4)	−0.00306(9)		0.0879(9)	
1082.349885(23)	7	4	A1	8	3	A2	^{R}P(8,3,A2)	5.22(1)	0.0620(2)	0.0597	0.802(5)	0.665(4)	−0.00306(9)		0.0879(9)	
1082.847607(20)	12	8	A1	13	9	A2	^{P}P(13,9,A2)	10.18(2)	0.0487(3)	0.0558	0.762(30)	0.618(1)	−0.00250(22)			
1083.497562(20)	11	6	E	12	7	E	^{P}P(12,7,E)	7.87(2)	0.0523(3)	0.0547	0.626(32)	0.614(1)	−0.00310(31)			
1084.418423(13)	10	4	E	11	5	E	^{P}P(11,5,E)	10.21(2)	0.0537(3)	0.0552	0.807(21)	0.620(1)	−0.00309(25)			
1085.228424(9)	7	3	E	8	2	E	^{R}P(8,2,E)	9.04(1)	0.0591(3)	0.0602	0.882(11)	0.670(4)			0.0881(6)	
1085.625324(8)	9	2	A2	10	3	A1	^{P}P(10,3,A1)	10.91(1)	0.0633(2)	0.0581	0.832(15)	0.649(2)		0.000027(2)	0.0893(8)	
1085.738824(8)	9	2	A1	10	3	A2	^{P}P(10,3,A2)	10.91(1)	0.0633(2)	0.0581	0.832(15)	0.649(2)		0.000027(2)	0.0893(8)	
1086.841190(42)	13	11	A2	14	12	A1	^{P}P(14,12,A1)	5.71(2)	0.0459(4)	0.0571		0.619(1)			0.0652(58)	
1087.149109(38)	12	9	E	13	10	E	^{P}P(13,10,E)	5.03(2)	0.0454(4)	0.0572		0.625(1)			0.0562(48)	
1087.570898(36)	11	7	E	12	8	E	^{P}P(12,8,E)	8.29(5)	0.0585(4)	0.0562	0.816(39)	0.624(1)	−0.00374(34)	0.000058(6)		
1087.887154(20)	6	5	E	7	4	E	^{R}P(7,4,E)	2.26(1)	0.0685(8)	0.0636		0.718(7)			0.0938(15)	
1088.082184(6)	7	2	E	8	1	E	^{R}P(8,1,E)	15.04(2)	0.0633(2)	0.0613	0.812(6)	0.682(5)	−0.00216(19)		0.0861(4)	
1088.252595(9)	10	5	A1	11	6	A2	^{P}P(11,6,A2)	22.65(3)	0.0527(1)	0.0553	0.712(10)	0.620(1)	−0.00307(11)			
1089.248131(10)	9	3	E	10	4	E	^{P}P(10,4,E)	13.36(2)	0.0565(2)	0.0569	0.755(13)	0.636(1)	−0.00351(19)			
1089.902710(5)	7	1	A2	8	0	A1	^{R}P(8,0,A1)	23.99(2)	0.0647(1)	0.0620	0.827(4)	0.690(5)	−0.00261(12)		0.0871(3)	
1090.645206(9)	8	1	E	9	2	E	^{P}P(9,2,E)	11.93(2)	0.0632(3)	0.0602	0.726(12)	0.671(3)	−0.00279(24)	0.000038(4)	0.0867(7)	
1090.725700(7)	6	4	A1	7	3	A2	^{R}P(7,3,A2)	9.87(1)	0.0656(3)	0.0618	0.792(7)	0.689(6)			0.094(5)	
1091.611499(38)	12	10	E	13	11	E	^{P}P(13,11,E)	5.21(2)	0.0462(4)	0.0580		0.630(1)				
1091.797634(12)	11	8	A2	12	9	A1	^{P}P(12,9,A1)	17.08(2)	0.0510(2)	0.0577	0.675(16)	0.635(1)	−0.00280(14)			
1092.239570(12)	10	6	E	11	7	E	^{P}P(11,7,E)	12.47(2)	0.0520(2)	0.0565	0.727(18)	0.631(1)				
1092.986295(9)	9	4	E	10	5	E	^{P}P(10,5,E)	15.69(2)	0.0557(2)	0.0562	0.751(12)	0.628(1)	−0.00245(16)	0.000036(3)		
1093.662989(7)	6	3	E	7	2	E	^{R}P(7,2,E)	8.98(1)	0.0620(2)	0.0616	0.813(7)	0.682(5)			0.0878(5)	
1094.044024(5)	8	2	A1	9	3	A2	^{P}P(9,3,A2)	16.06(1)	0.0642(2)	0.0590	0.774(6)	0.658(3)	−0.00214(11)	0.000023(1)	0.0893(4)	
1094.117524(5)	8	2	A2	9	3	A1	^{P}P(9,3,A1)	16.06(1)	0.0642(2)	0.0590	0.774(6)	0.658(3)	−0.00214(11)	0.000023(1)	0.0893(4)	
1095.705469(8)	7	0	E	8	1	E	^{P}P(8,1,E)	9.59(2)	0.0652(3)	0.0620	0.792(9)	0.689(5)	−0.00381(25)		0.0858(14)	0.788(18)
1096.184869(20)	11	9	E	12	10	E	^{P}P(12,10,E)	8.71(2)	0.0507(2)	0.0588		0.643(1)	−0.00110(0)			
1096.378207(12)	10	7	E	11	8	E	^{P}P(11,8,E)	13.36(2)	0.0522(2)	0.0582	0.677(15)	0.645(1)	−0.00340(15)			
1096.631621(5)	6	2	E	7	1	E	^{R}P(7,1,E)	15.86(2)	0.0632(1)	0.0626	0.822(4)	0.693(6)	−0.00160(14)		0.0846(6)	0.772(7)
1096.879089(6)	9	5	A1	10	6	A2	^{P}P(10,6,A2)	35.63(3)	0.0545(1)	0.0569	0.762(5)	0.635(1)	−0.00271(6)	0.000012(1)	0.0777(8)	0.696(23)
1097.713516(7)	8	3	E	9	4	E	^{P}P(9,4,E)	19.9(2)	0.0574(1)	0.0578	0.801(6)	0.643(2)	−0.00264(11)	0.000013(1)	0.0788(9)	0.763(19)
1098.725853(5)	6	1	A1	7	0	A2	^{R}P(7,0,A2)	28.66(2)	0.0650(1)	0.0633	0.829(2)	0.701(6)	−0.00223(8)	0.000016(1)	0.0852(4)	0.788(4)
1098.933992(6)	7	1	E	8	2	E	^{P}P(8,2,E)	17.10(2)	0.0628(2)	0.0613	0.821(6)	0.681(4)	−0.00207(14)	0.000024(2)	0.0820(7)	0.784(12)
1099.005454(7)	5	4	A2	6	3	A1	^{R}P(6,3,A1)	7.32(1)	0.0693(3)	0.0643	0.804(6)	0.720(7)	−0.00294(20)	0.000051(5)	0.0894(13)	0.761(12)
1100.672437(8)	10	8	A2	11	9	A1	^{P}P(11,9,A1)	27.42(3)	0.0512(1)	0.0596	0.750(8)	0.656(1)	−0.00255(8)	0.000024(2)	0.0767(6)	
1100.743446(20)	11	10	E	12	11	E	^{P}P(12,11,E)	8.80(2)	0.0434(2)	0.0589	0.660(29)	0.645(1)	−0.00262(18)			
1100.921805(8)	9	6	E	10	7	E	^{P}P(10,7,E)	19.25(2)	0.0545(1)	0.0587	0.709(9)	0.653(2)	−0.00226(10)	0.000032(2)	0.0815(7)	
1101.505850(6)	8	4	E	9	5	E	^{P}P(9,5,E)	23.28(2)	0.0569(1)	0.0577	0.775(6)	0.641(2)	−0.00247(9)	0.000021(2)	0.0787(8)	0.771(18)
1101.981493(6)	5	3	E	6	2	E	^{R}P(6,2,E)	7.95(1)	0.0642(2)	0.0633	0.834(5)	0.699(6)			0.0885(5)	
1102.423989(4)	7	2	A2	8	3	A1	^{P}P(8,3,A1)	22.84(1)	0.0655(2)	0.0600	0.779(8)	0.666(4)	−0.00215(7)	0.000025(1)	0.0859(2)	0.796(26)
1102.468792(4)	7	2	A1	8	3	A2	^{P}P(8,3,A2)	22.84(1)	0.0655(2)	0.0600	0.779(8)	0.666(4)	−0.00215(7)	0.000025(1)	0.0859(2)	0.796(26)
1103.850673(6)	6	0	E	7	1	E	^{P}P(7,1,E)	13.84(2)	0.0655(2)	0.0633	0.816(5)	0.701(6)	−0.00189(17)	0.000021(3)	0.0890(8)	0.750(8)
1105.032601(5)	5	2	E	6	1	E	^{R}P(6,1,E)	15.20(2)	0.0645(2)	0.0639	0.832(3)	0.703(6)	−0.00276(16)		0.0861(6)	0.767(6)
1105.115847(14)	9	7	E	10	8	E	^{P}P(10,8,E)	20.64(4)	0.0537(3)	0.0604	0.733(19)	0.669(2)	−0.00236(20)			0.912(25)
1105.130058(21)	10	9	E	11	10	E	^{P}P(11,10,E)	14.16(4)	0.0480(3)	0.0599	0.716(37)	0.660(1)			0.0773(25)	

1105.447409(6)	8	5	A1	9	6	A2	^{P}P(9,6,A2)	52.73(4)	0.057(1)	0.0591	0.765(3)	0.659(3)	−0.00284(6)	0.000014(1)	0.0778(5)	0.804(11)
1105.490676(14)	11	11	A1	12	12	A2	^{P}P(12,12,A2)	17.12(3)	0.0269(1)	0.0558	0.375(19)	0.634(1)	−0.00514(7)	0.000029(2)		
1106.132104(6)	7	3	E	8	4	E	^{P}P(8,4,E)	28.56(2)	0.0593(1)	0.0591	0.812(4)	0.653(3)	−0.0033(8)	0.000017(1)	0.0781(5)	0.809(9)
1107.190909(20)	4	4	A1	5	3	A2	^{R}P(5,3,A2)	3.62(2)	0.0760(14)	0.0669		0.748(7)		0.000030(2)		
1107.196929(12)	6	1	E	7	2	E	^{P}P(7,2,E)	22.91(4)	0.0627(2)	0.0624	0.801(5)	0.691(6)	−0.00258(11)	0.000019(2)	0.0879(7)	0.738(7)
1107.406665(5)	5	1	A2	6	0	A1	^{R}P(6,0,A1)	32.60(2)	0.0665(1)	0.0647	0.841(1)	0.711(6)	−0.00288(7)	0.000019(1)	0.0861(3)	0.775(3)
1109.465904(7)	9	8	A1	10	9	A2	^{P}P(10,9,A2)	43.05(4)	0.0500(1)	0.0609	0.726(5)	0.676(2)	−0.00207(6)	0.000023(1)	0.0750(9)	0.753(26)
1109.536457(7)	8	6	E	9	7	E	^{P}P(9,7,E)	29.08(4)	0.0565(1)	0.0610	0.768(6)	0.680(3)	−0.00218(9)	0.000019(2)	0.0788(8)	0.804(18)
1109.761551(14)	10	10	E	11	11	E	^{P}P(11,11,E)	14.36(2)	0.0301(1)	0.0568	0.510(14)	0.647(1)	−0.00435(9)	0.000041(2)		
1109.967774(6)	7	4	E	8	5	E	^{P}P(8,5,E)	33.02(3)	0.0588(1)	0.0598	0.790(3)	0.664(3)	−0.00137(8)	0.000028(1)	0.0821(5)	0.761(8)
1110.192698(6)	4	3	E	5	2	E	^{R}P(5,2,E)	5.81(1)	0.0741(2)	0.0654		0.724(6)	−0.00362(36)		0.0908(4)	
1110.754522(7)	6	2	A1	7	3	A2	^{P}P(7,3,A2)	30.93(1)	0.0645(1)	0.0612	0.805(1)	0.675(5)	−0.00218(4)	0.000026(1)	0.0871(1)	0.787(1)
1110.779654(12)	6	2	A2	7	3	A1	^{P}P(7,3,A1)	30.93(1)	0.0645(1)	0.0612	0.805(1)	0.675(5)	−0.00218(4)	0.000026(1)	0.0871(1)	0.787(1)
1111.988897(5)	5	0	E	6	1	E	^{P}P(6,1,E)	18.51(2)	0.0656(1)	0.0647	0.849(2)	0.711(6)	−0.00204(14)	0.000016(2)	0.0870(5)	0.772(5)
1113.297730(5)	4	2	E	5	1	E	^{R}P(5,1,E)	12.88(2)	0.0645(2)	0.0655	0.861(2)	0.717(6)	−0.00314(17)		0.0896(6)	0.755(5)
1113.776358(7)	8	7	E	9	8	E	^{P}P(9,8,E)	31.26(3)	0.0540(1)	0.0618	0.730(5)	0.691(4)	−0.00262(8)			
1113.948879(5)	7	5	A2	8	6	A1	^{P}P(8,6,A1)	75.51(5)	0.0594(1)	0.0616	0.781(2)	0.688(4)	−0.00259(6)	0.000009(1)	0.0803(3)	0.795(5)
1113.979823(10)	9	9	E	10	10	E	^{P}P(10,10,E)	22.52(5)	0.0342(1)	0.0578	0.534(12)	0.660(1)	−0.00467(9)	0.000031(2)	0.0539(19)	0.669(65)
1114.493311(5)	6	3	E	7	4	E	^{P}P(7,4,E)	38.27(2)	0.0609(1)	0.0609	0.816(2)	0.672(4)	−0.00270(7)	0.000015(1)	0.0816(3)	0.779(4)
1115.420049(5)	5	1	E	6	2	E	^{P}P(6,2,E)	29.34(2)	0.0634(1)	0.0638	0.835(2)	0.701(6)	−0.00214(8)	0.000021(1)	0.0848(4)	0.786(4)
1115.940928(5)	4	1	A1	5	0	A2	^{R}P(5,0,A1)	33.58(2)	0.0669(1)	0.0663	0.856(1)	0.723(6)	−0.00241(8)	0.000011(1)	0.0878(3)	0.774(3)
1118.076223(5)	7	6	E	8	7	E	^{P}P(8,7,E)	41.80(3)	0.0568(1)	0.0627	0.760(3)	0.703(5)	−0.00215(6)	0.000014(1)	0.0793(4)	0.766(9)
1118.172377(5)	8	8	A1	9	9	A2	^{P}P(9,9,A2)	65.54(3)	0.0385(0)	0.0588	0.547(3)	0.675(2)	−0.00374(3)	0.000033(1)	0.0588(5)	0.697(16)
1118.304501(7)	3	3	E	4	2	E	^{R}P(4,2,E)	2.87(0)	0.0782(10)	0.0677	0.770(15)	0.749(7)	−0.00730(61)		0.0873(26)	0.806(23)
1118.363421(4)	6	4	E	7	5	E	^{P}P(7,5,E)	45.26(3)	0.0610(1)	0.0623	0.822(3)	0.694(5)	−0.00233(6)	0.000015(1)	0.0838(3)	0.773(4)
1119.025382(8)	5	2	A2	6	3	A1	^{P}P(6,3,A1)	40.05(1)	0.0675(0)	0.0627	0.814(1)	0.688(5)	−0.00210(3)	0.000023(2)	0.0925(1)	0.761(1)
1119.038034(12)	5	2	A1	6	3	A2	^{P}P(6,3,A2)	40.05(1)	0.0675(0)	0.0627	0.814(1)	0.688(5)	−0.00210(3)	0.000023(2)	0.0925(1)	0.761(1)
1120.103181(4)	4	0	E	5	1	E	^{P}P(5,1,E)	22.67(2)	0.0663(1)	0.0663	0.850(2)	0.722(6)	−0.00250(11)	0.000013(1)	0.0887(4)	0.761(3)
1121.441410(5)	3	2	E	4	1	E	^{R}P(4,1,E)	9.24(1)	0.0662(2)	0.0671	0.853(4)	0.734(6)	−0.00233(14)		0.0911(8)	0.739(6)
1122.353699(6)	7	7	E	8	8	E	^{P}P(8,8,E)	44.77(7)	0.0426(1)	0.0599	0.629(6)	0.690(3)	−0.00319(8)	0.000026(1)	0.0638(5)	0.745(14)
1122.376165(4)	6	5	A2	7	6	A1	^{P}P(7,6,A1)	105.06(7)	0.0604(1)	0.0636	0.789(2)	0.714(6)	−0.00207(5)	0.000017(1)	0.0806(2)	0.784(3)
1122.788184(4)	5	3	E	6	4	E	^{P}P(6,4,E)	49.73(2)	0.0634(1)	0.0631	0.825(2)	0.699(5)	−0.00273(5)	0.000010(1)	0.0835(3)	0.781(3)
1123.589807(4)	4	1	E	5	2	E	^{P}P(5,2,E)	35.43(2)	0.0640(1)	0.0652	0.842(2)	0.713(6)	−0.00308(7)	0.000014(1)	0.0857(3)	0.772(3)
1124.325714(4)	3	1	A2	4	0	A1	^{R}P(4,0,A1)	31.36(2)	0.0673(1)	0.0679	0.860(1)	0.735(6)	−0.00284(8)	0.000010(1)	0.0896(3)	0.765(3)
1126.534176(6)	6	6	E	7	7	E	^{P}P(7,7,E)	58.571(4)	0.0488(1)	0.0611	0.680(2)	0.704(5)	−0.00313(4)	0.000030(1)	0.0706(6)	0.668(18)
1126.684492(6)	5	4	E	6	5	E	^{P}P(6,5,E)	59.77(3)	0.0623(1)	0.0645	0.805(2)	0.721(6)	−0.00243(5)	0.000009(1)	0.0807(6)	0.871(18)
1127.227037(20)	4	2	A1	5	3	A2	^{P}P(5,3,A2)	48.64(1)	0.0643(0)	0.0645	0.822(1)	0.709(6)	−0.00251(4)	0.000015(2)	0.0737(9)	
1127.232695(14)	4	2	A2	5	3	A1	^{P}P(5,3,A1)	48.64(1)	0.0643(0)	0.0645	0.822(1)	0.709(6)	−0.00251(4)	0.000015(2)	0.0737(9)	
1128.174506(6)	3	0	E	4	1	E	^{P}P(4,1,E)	25.18(2)	0.0674(1)	0.0679	0.836(2)	0.734(6)	−0.00224(10)	0.000013(1)	0.0839(2)	
1129.139102(28)	10	9	E	10	8	E	^{R}Q(10,8,E)	3.84(1)	0.0615(5)	0.0611		0.684(4)	−0.00498(40)			
1129.476960(11)	2	2	E	3	1	E	^{R}P(3,1,E)	4.62(1)	0.0762(3)	0.0689		0.753(7)	−0.00189(17)			
1130.486989(25)	11	8	E	11	7	E	^{R}Q(11,7,E)	4.89(2)	0.0558(5)	0.0576	0.522(43)	0.644(1)				
1130.561033(30)	13	7	A2	13	6	A1	^{R}Q(13,6,A1)	5.63(2)	0.0509(4)	0.0532	0.549(51)	0.605(1)		0.000065(6)		
1130.721975(5)	5	5	A2	6	6	A1	^{P}P(6,6,A1)	140.05(4)	0.0537(1)	0.0623	0.724(1)	0.716(5)	−0.00289(3)	0.000024(2)	0.0707(3)	0.806(11)
1131.008024(20)	4	3	E	5	4	E	^{P}P(5,4,E)	62.37(2)	0.0647(1)	0.0653	0.822(1)	0.728(6)	−0.00228(6)	0.000010(1)	0.0837(6)	0.828(17)
1131.434300(19)	10	8	E	10	7	E	^{R}Q(10,7,E)	6.00(2)	0.0597(4)	0.0598	0.558(29)	0.669(3)	−0.00477(38)			
1131.693962(6)	3	1	E	4	2	E	^{P}P(4,2,E)	40.36(2)	0.0644(1)	0.0668	0.846(1)	0.727(6)	−0.00292(7)	0.000014(1)	0.0836(9)	0.818(24)
1131.766548(18)	12	7	A2	12	6	A1	^{R}Q(12,6,A1)	8.54(2)	0.0521(3)	0.0543	0.748(31)	0.614(1)	−0.00291(25)			
1132.557787(6)	2	1	A1	3	0	A2	^{R}P(3,0,A2)	24.95(2)	0.0667(1)	0.0695	0.869(2)	0.749(6)	−0.00335(16)	0.000012(1)	0.0919(2)	
1132.858722(13)	11	7	A2	11	6	A1	^{R}Q(11,6,A1)	12.16(3)	0.0561(5)	0.0559	0.582(26)	0.629(1)				
1133.033465(17)	8	8	E	8	7	E	^{R}Q(8,7,E)	4.79(1)	0.0695(5)	0.0628		0.719(6)	−0.00978(64)			
1133.841173(10)	10	7	A2	10	6	A1	^{R}Q(10,6,A1)	15.93(3)	0.0571(3)	0.0580	0.714(16)	0.650(2)				
1134.717981(8)	9	7	A1	9	6	A2	^{R}Q(9,6,A2)	19.06(3)	0.0597(3)	0.0603	0.748(11)	0.677(3)				
1134.923731(6)	4	4	E	5	5	E	^{P}P(5,5,E)	76.54(3)	0.0582(1)	0.0635	0.747(2)	0.727(6)	−0.00182(7)	0.000027(1)	0.0354(7)	

Table 5 (*continued*)

Position, cm^{-1}	J′	K′	S′	J″	K″	S″	Assignment	Int*10[25a]	$b_L^0(N_2)$ expt,[b]	$b_L^0(N_2)$ calc.[b]	n_1 expt	n_1 calc.	$\delta^0(N_2)$ expt[b]	$\delta'(N_2)$ expt[c]	$b_L^0(self)$ expt[b]	n_2 expt
1135.352143(22)	3	2	A2	4	3	A1	^{P}P(4,3,A1)	114.47(3)	0.0653(1)	0.0664	0.852(1)	0.733(6)	−0.00225(13)	0.000012(1)	0.0857(1)	
1135.493275(8)	8	7	A2	8	6	A1	^{R}Q(8,6,A1)	19.18(5)	0.0628(3)	0.0626	0.821(10)	0.705(5)	−0.0036(36)		0.0841(6)	
1136.171086(19)	7	7	A1	7	6	A2	^{R}Q(7,6,A2)	14.28(5)	0.0697(6)	0.0638	0.764(17)	0.728(7)			0.0868(16)	
1136.185383(14)	2	0	E	3	1	E	^{P}P(3,1,E)	25.02(2)	0.0668(2)	0.0695	0.855(3)	0.748(6)			0.0910(5)	
1136.350725(13)	10	6	E	10	5	E	^{R}Q(10,5,E)	9.78(2)	0.0572(5)	0.0563	0.642(25)	0.633(1)				
1137.263915(10)	9	6	E	9	5	E	^{R}Q(9,5,E)	12.53(2)	0.0585(4)	0.0584	0.818(16)	0.655(2)				
1137.869412(20)	11	5	E	11	4	E	^{R}Q(11,4,E)	7.64(2)	0.0546(3)	0.0550	0.739(23)	0.620(1)			0.0753(25)	
1138.068790(9)	8	6	E	8	5	E	^{R}Q(8,5,E)	14.15(2)	0.0620(1)	0.0608		0.683(4)	−0.00187(13)		0.0869(6)	
1138.770173(8)	7	6	E	7	5	E	^{R}Q(7,5,E)	14.16(2)	0.0664(1)	0.0633		0.712(6)	−0.00255(13)	0.000020(1)	0.0874(5)	
1138.949449(13)	10	5	E	10	4	E	^{R}Q(10,4,E)	11.08(2)	0.0574(2)	0.0559	0.651(14)	0.628(1)			0.0795(14)	
1139.112237(35)	3	3	E	4	4	E	^{P}P(4,4,E)	4.81(2)	0.0529(4)	0.0649	0.830(8)	0.737(6)				
1139.372679(12)	6	6	E	6	5	E	^{R}Q(6,5,E)	9.95(2)	0.0679(3)	0.0647	0.844(7)	0.735(7)	−0.00491(26)	0.000042(4)	0.096(13)	0.707(12)
1139.722075(6)	2	1	E	3	2	E	^{P}P(3,2,E)	43.46(2)	0.0649(1)	0.0682	0.854(1)	0.745(6)	−0.00203(6)	0.000022(1)	0.0883(1)	
1139.909156(11)	9	5	E	9	4	E	^{R}Q(9,4,E)	14.64(2)	0.0578(2)	0.0572	0.716(9)	0.639(1)			0.0866(8)	
1140.391680(21)	11	4	A1	11	3	A2	^{R}Q(11,3,A2)	7.11(2)	0.0602(4)	0.0559	0.760(35)	0.628(1)	0.00427(41)		0.0850(27)	
1140.427310(20)	11	4	A2	11	3	A1	^{R}Q(11,3,A1)	7.50(2)	0.0598(4)	0.0559	0.707(33)	0.628(1)	−0.00522(38)		0.0848(26)	
1140.634587(6)	1	1	A2	2	0	A1	^{R}P(2,0,A1)	14.39(1)	0.0664(1)	0.0710	0.839(2)	0.764(6)	−0.00318(15)	0.000024(1)	0.0919(1)	
1140.752289(8)	8	5	E	8	4	E	^{R}Q(8,4,E)	18.20(2)	0.0603(1)	0.0590		0.659(3)	−0.00082(8)		0.0819(4)	
1141.483940(6)	7	5	E	7	4	E	^{R}Q(7,4,E)	20.29(3)	0.0638(1)	0.0615	0.786(4)	0.687(5)	−0.00220(13)	0.000011(1)	0.0866(3)	
1141.562032(14)	10	4	A2	10	3	A1	^{R}Q(10,3,A1)	10.67(2)	0.0623(3)	0.0566	0.699(21)	0.635(1)				
1141.597406(13)	10	4	A1	10	3	A2	^{R}Q(10,3,A2)	11.42(2)	0.0598(3)	0.0566	0.780(19)	0.635(1)	−0.00574(26)			
1142.109752(6)	6	5	E	6	4	E	^{R}Q(6,4,E)	19.43(2)	0.0663(1)	0.0640	0.819(4)	0.718(6)	−0.00323(12)	0.000016(2)	0.0909(3)	
1142.582166(11)	9	4	A1	9	3	A2	^{R}Q(9,3,A2)	14.07(3)	0.0634(2)	0.0575	0.801(9)	0.642(2)	0.00366(9)		0.0819(13)	0.850(19)
1142.628435(19)	9	4	A2	9	3	A1	^{R}Q(9,3,A1)	15.86(6)	0.0634(2)	0.0575	0.801(9)	0.642(2)	0.00366(9)		0.0819(13)	0.850(19)
1142.635080(9)	5	5	E	5	4	E	^{R}Q(5,4,E)	13.68(4)	0.0680(3)	0.0657	0.87(8)	0.742(7)	−0.01596(25)		0.0935(4)	
1143.391181(6)	2	2	A1	3	3	A2	^{P}P(3,3,A2)	131.69(3)	0.0656(0)	0.0665	0.832(1)	0.746(6)	−0.00248(4)	0.000017(2)	0.0853(2)	0.787(2)
1143.527523(7)	8	4	A1	8	3	A2	^{R}Q(8,3,A2)	20.88(2)	0.0653(1)	0.0586	0.785(3)	0.652(3)	−0.00174(6)		0.0878(2)	
1143.571633(8)	8	4	A2	8	3	A1	^{R}Q(8,3,A1)	19.27(3)	0.0653(1)	0.0586	0.785(3)	0.652(3)	−0.00174(6)		0.0878(2)	
1144.121476(6)	1	0	E	2	1	E	^{P}P(2,1,E)	22.36(2)	0.0662(1)	0.0709	0.861(2)	0.763(6)	−0.0029(10)	0.000020(1)	0.0924(4)	0.741(4)
1144.218243(14)	10	3	E	10	2	E	^{R}Q(10,2,E)	9.88(2)	0.0602(3)	0.0578	0.829(18)	0.646(1)	−0.00249(24)			
1144.302129(14)	7	4	A2	7	3	A1	^{R}Q(7,3,A1)	25.11(2)	0.0619(1)	0.0602	0.811(1)	0.667(4)	−0.00107(5)	0.000007(1)	0.0838(6)	0.762(5)
1144.307543(14)	7	4	A1	7	3	A2	^{R}Q(7,3,A2)	25.11(2)	0.0619(1)	0.0602	0.811(1)	0.667(4)	−0.00107(5)	0.000007(1)	0.0838(6)	0.762(5)
1144.960590(5)	6	4	A1	6	3	A2	^{R}Q(6,3,A2)	54.31(3)	0.0641(1)	0.0624	0.825(2)	0.692(6)	−0.00170(5)		0.0873(5)	0.816(12)
1145.360462(8)	9	3	E	9	2	E	^{R}Q(9,2,E)	14.55(3)	0.0607(2)	0.0586	0.756(9)	0.655(2)	−0.00201(15)		0.0841(7)	
1145.508861(5)	5	4	A2	5	3	A1	^{R}Q(5,3,A1)	50.63(2)	0.0671(1)	0.0648	0.842(1)	0.722(6)	−0.00221(6)	0.000015(1)	0.0908(2)	
1145.955000(5)	4	4	A1	4	3	A2	^{R}Q(4,3,A2)	34.56(2)	0.0705(1)	0.0668	0.864(1)	0.747(7)	−0.00373(8)	0.000024(1)	0.0956(2)	
1146.350463(6)	8	3	E	8	2	E	^{R}Q(8,2,E)	20.22(2)	0.0591(1)	0.0595	0.812(5)	0.663(3)	−0.00155(10)		0.0862(4)	
1146.564067(18)	10	2	E	10	1	E	^{R}Q(10,1,E)	5.12(1)	0.0618(4)	0.0587	0.813(28)	0.655(2)				
1147.196047(6)	7	3	E	7	2	E	^{R}Q(7,2,E)	26.37(2)	0.0606(1)	0.0607	0.813(3)	0.672(4)	−0.00073(6)	0.000011(1)	0.0850(3)	
1147.665833(5)	1	1	E	2	2	E	^{P}P(2,2,E)	45.26(2)	0.0665(1)	0.0684	0.859(1)	0.757(6)	−0.00221(6)	0.000017(1)	0.0933(5)	0.755(10)
1147.906526(8)	6	3	E	6	2	E	^{R}Q(6,2,E)	32.07(3)	0.0633(1)	0.0621	0.834(3)	0.684(5)			0.0893(10)	0.703(20)
1148.492390(5)	5	3	E	5	2	E	^{R}Q(5,2,E)	33.82(2)	0.0651(1)	0.0639	0.832(2)	0.703(6)	−0.00182(7)	0.000009(1)	0.0868(2)	
1148.963335(5)	4	3	E	4	2	E	^{R}Q(4,2,E)	30.82(2)	0.0666(1)	0.0660	0.849(2)	0.728(6)	−0.00184(8)	0.000014(1)	0.0897(2)	
1149.063784(7)	8	2	E	8	1	E	^{R}Q(8,1,E)	13.87(2)	0.0644(2)	0.0607	0.780(8)	0.677(4)			0.0879(6)	
1149.328536(5)	3	3	E	3	2	E	^{R}Q(3,2,E)	20.75(2)	0.0697(1)	0.0678	0.873(2)	0.752(6)	−0.00275(12)	0.000018(1)	0.0956(3)	
1150.055828(6)	7	2	E	7	1	E	^{R}Q(7,1,E)	20.49(2)	0.0631(1)	0.0618	0.839(4)	0.686(5)		0.000011(2)	0.0866(3)	
1150.880549(5)	6	2	E	6	1	E	^{R}Q(6,1,E)	27.63(2)	0.0633(1)	0.0631	0.835(2)	0.696(6)	−0.00147(8)		0.0883(2)	
1151.547989(5)	5	2	E	5	1	E	^{R}Q(5,1,E)	33.79(2)	0.0645(1)	0.0646	0.83(2)	0.707(6)	−0.00158(7)		0.0881(2)	
1151.972417(6)	0	0	E	1	1	E	^{P}P(1,1,E)	16.39(2)	0.0657(1)	0.0720	0.834(2)	0.773(6)	−0.00267(13)	0.000021(1)	0.0957(3)	

1152.072139(5)	4	2	E	4	1	E	^{R}Q(4,1,E)	36.78(2)	0.0649(1)	0.0662	0.855(1)	0.721(6)	−0.00191(7)		0.0883(2)	
1152.468500(5)	3	2	E	3	1	E	^{R}Q(3,1,E)	33.77(2)	0.0653(1)	0.0678	0.850(1)	0.739(6)	−0.00241(7)	0.000014(1)	0.0889(2)	
1152.751674(5)	2	2	E	2	1	E	^{R}Q(2,1,E)	22.87(1)	0.0663(1)	0.0692	0.864(1)	0.757(6)	−0.0023(10)	0.000019(1)	0.0930(2)	
1154.43943(16)	13	1	A1	13	0	A2	^{R}Q(13,0,A2)	15.64(3)	0.0590(2)	0.0564	0.84(19)	0.623(1)	−0.00186(12)	0.000018(3)	0.0891(21)	
1154.713917(12)	12	1	A2	12	0	A1	^{R}Q(12,0,A1)	22.1(3)	0.0591(2)	0.0573	0.87(12)	0.634(1)	−0.00135(11)		0.0661(9)	
1154.966470(9)	11	1	A1	11	0	A2	^{R}Q(11,0,A2)	32.63(5)	0.0603(1)	0.0582	0.769(7)	0.646(1)	−0.00158(9)	0.000013(2)	0.0843(6)	
1155.070691(21)	13	0	E	13	1	E	^{P}Q(13,1,E)	10.78(3)	0.0606(3)	0.0564	0.634(30)	0.623(1)			0.0774(28)	
1155.199670(8)	10	1	A2	10	0	A1	^{R}Q(10,0,A1)	44.83(4)	0.0618(1)	0.0592	0.776(4)	0.659(2)	−0.00110(7)	0.000016(1)	0.0826(4)	
1155.422423(7)	9	1	A1	9	0	A2	^{R}Q(9,0,A2)	55.81(5)	0.0625(1)	0.0603	0.790(3)	0.672(3)	−0.00116(7)		0.0833(3)	
1155.521843(7)	8	1	A2	8	0	A1	^{R}Q(8,0,A1)	64.88(5)	0.0650(1)	0.0614	0.822(3)	0.684(4)	−0.00267(7)	0.000018(1)	0.0855(3)	
1155.594148(12)	12	0	E	12	1	E	^{P}Q(12,1,E)	21.25(4)	0.0601(2)	0.0573	0.768(17)	0.634(1)	−0.00133(10)		0.0806(12)	
1155.728731(7)	7	1	A1	7	0	A2	^{R}Q(7,0,A2)	89.9(5)	0.0649(1)	0.0626	0.824(2)	0.695(5)	−0.00203(5)	0.000016(1)	0.0851(2)	
1155.879355(7)	6	1	A2	6	0	A1	^{R}Q(6,0,A1)	102.37(6)	0.0655(1)	0.0639	0.831(1)	0.705(6)	−0.00146(6)	0.000013(1)	0.0860(2)	
1156.004835(13)	5	1	A1	5	0	A2	^{R}Q(5,0,A2)	107.72(10)	0.0659(1)	0.0654	0.828(1)	0.715(6)	−0.00186(6)	0.000007(1)	0.0841(3)	
1156.108549(7)	4	1	A2	4	0	A1	^{R}Q(4,0,A1)	107.76(7)	0.0660(1)	0.0670	0.855(1)	0.727(6)	−0.00206(6)	0.000005(1)	0.0872(2)	
1156.191028(7)	3	1	A1	3	0	A2	^{R}Q(3,0,A2)	97.04(8)	0.0660(1)	0.0687	0.840(2)	0.740(6)	−0.00190(7)		0.0876(2)	
1156.252680(8)	2	1	A2	2	0	A1	^{R}Q(2,0,A1)	77.66(9)	0.0666(1)	0.0702	0.820(2)	0.755(6)	−0.00248(9)	0.000009(1)	0.0869(8)	0.814(20)
1156.293622(11)	1	1	A1	1	0	A2	^{R}Q(1,0,A2)	49.68(7)	0.0671(1)	0.0716	0.758(2)	0.770(6)	−0.00354(9)	0.000014(1)	0.0892(3)	
1156.424297(8)	10	0	E	10	1	E	^{P}Q(10,1,E)	39.85(4)	0.0614(1)	0.0592	0.802(6)	0.659(2)	−0.00164(7)		0.0830(4)	
1156.658762(37)	14	1	E	14	2	E	^{P}Q(14,2,E)	8.40(4)	0.0582(3)	0.0553		0.612(1)			0.0794(46)	
1156.836955(8)	9	0	E	9	1	E	^{P}Q(9,1,E)	50.63(4)	0.0623(1)	0.0603	0.804(3)	0.672(3)	−0.00168(6)	0.000007(1)	0.0836(3)	
1157.255809(11)	8	0	E	8	1	E	^{P}Q(8,1,E)	60.80(7)	0.0632(1)	0.0614	0.807(3)	0.684(4)	−0.0016(10)		0.0849(3)	
1157.272717(28)	13	1	E	13	2	E	^{P}Q(13,2,E)	13.02(5)	0.0612(4)	0.0561	0.865(50)	0.622(1)			0.0783(36)	
1157.679116(7)	7	0	E	7	1	E	^{P}Q(7,1,E)	68.21(4)	0.0646(1)	0.0626	0.815(2)	0.695(5)	−0.00171(5)	0.000010(1)	0.0802(8)	0.883(24)
1157.885570(41)	12	1	E	12	2	E	^{P}Q(12,2,E)	18.58(3)	0.0596(2)	0.0569	0.720(14)	0.631(1)	−0.00221(14)			
1158.099455(8)	6	0	E	6	1	E	^{P}Q(6,1,E)	71.64(4)	0.0657(1)	0.0639	0.807(2)	0.705(6)	−0.00196(5)	0.000008(1)	0.0810(9)	0.898(25)
1158.504362(9)	5	0	E	5	1	E	^{P}Q(5,1,E)	71.38(3)	0.0690(1)	0.0654	0.792(1)	0.715(6)	−0.00186(5)	0.000007(1)	0.0821(12)	0.877(33)
1158.877568(7)	4	0	E	4	1	E	^{P}Q(4,1,E)	64.98(3)	0.0663(1)	0.0670	0.839(1)	0.727(6)	−0.00183(5)		0.0826(9)	0.882(24)
1159.116825(9)	10	1	E	10	2	E	^{P}Q(10,2,E)	34.05(5)	0.0612(1)	0.0587	0.770(7)	0.655(2)	−0.00248(9)	0.000022(2)	0.0792(4)	
1159.201560(8)	3	0	E	3	1	E	^{P}Q(3,1,E)	54.72(3)	0.0662(1)	0.0687	0.840(1)	0.740(6)	−0.00226(6)	0.000013(1)	0.0879(2)	
1159.460170(8)	2	0	E	2	1	E	^{P}Q(2,1,E)	41.65(2)	0.0664(1)	0.0702	0.840(1)	0.755(6)	−0.00236(7)		0.0883(2)	
1159.513193(34)	14	2	A2	14	3	A1	^{P}Q(14,3,A1)	7.37(3)	0.0572(4)	0.0549	0.697(56)	0.610(1)			0.0672(45)	
1159.640105(8)	1	0	E	1	1	E	^{P}Q(1,1,E)	25.71(2)	0.0668(1)	0.0716	0.832(1)	0.770(6)	−0.00377(13)	0.000026(1)	0.0937(22)	0.656(53)
1159.728243(8)	9	1	E	9	2	E	^{P}Q(9,2,E)	41.49(4)	0.0604(1)	0.0597	0.827(4)	0.666(3)	−0.00260(7)	0.000021(1)	0.0876(13)	0.670(34)
1159.810303(21)	13	2	A2	13	3	A1	^{P}Q(13,3,A1)	11.23(3)	0.0604(3)	0.0555	0.924(31)	0.619(1)				
1160.326721(7)	8	1	E	8	2	E	^{P}Q(8,2,E)	49.84(4)	0.0618(1)	0.0607	0.805(2)	0.677(4)	−0.00244(6)	0.000014(1)	0.0840(2)	
1160.638984(13)	12	2	A1	12	3	A2	^{P}Q(12,3,A2)	16.19(2)	0.0611(1)	0.0562		0.627(1)			0.0852(12)	
1160.901607(7)	7	1	E	7	2	E	^{P}Q(7,2,E)	56.15(3)	0.0627(1)	0.0618	0.813(2)	0.686(5)	−0.00259(6)	0.000015(1)	0.0839(2)	
1160.958662(14)	12	2	A2	12	3	A1	^{P}Q(12,3,A1)	16.19(2)	0.0611(1)	0.0562		0.627(1)			0.0852(12)	
1161.440596(8)	6	1	E	6	2	E	^{P}Q(6,2,E)	59.47(3)	0.0640(1)	0.0631	0.818(2)	0.696(6)	−0.00153(6)	0.000018(1)	0.0858(2)	
1161.685867(9)	10	4	E	10	5	E	^{P}Q(10,5,E)	22.04(3)	0.0617(2)	0.0559	0.766(9)	0.628(1)	−0.00299(13)	0.000041(3)	0.0871(8)	
1161.930961(6)	5	1	E	5	2	E	^{P}Q(5,2,E)	58.61(2)	0.0645(1)	0.0646	0.833(1)	0.707(6)	−0.00229(6)	0.000014(1)	0.0811(8)	0.907(23)
1162.239713(9)	10	2	A1	10	3	A2	^{P}Q(10,3,A2)	29.52(3)	0.0628(1)	0.0578	0.787(4)	0.646(1)	−0.00217(7)		0.0828(4)	
1162.360469(7)	4	1	E	4	2	E	^{P}Q(4,2,E)	53.94(3)	0.0649(1)	0.0662	0.860(1)	0.721(6)	−0.00289(6)	0.000010(1)	0.0869(2)	
1162.406376(8)	10	2	A2	10	3	A1	^{P}Q(10,3,A1)	29.52(3)	0.0628(1)	0.0578	0.787(4)	0.646(1)	−0.00217(7)		0.0839(2)	
1162.718028(7)	3	1	E	3	2	E	^{P}Q(3,2,E)	43.17(2)	0.0660(1)	0.0678	0.857(1)	0.739(6)	−0.00155(7)	0.000013(1)	0.0878(2)	
1162.994624(9)	2	1	E	2	2	E	^{P}Q(2,2,E)	26.68(2)	0.0672(1)	0.0692	0.871(2)	0.757(7)		0.000020(1)	0.0909(4)	
1162.997143(10)	9	2	A2	9	3	A1	^{P}Q(9,3,A1)	36.84(5)	0.0639(1)	0.0586	0.778(2)	0.655(2)	−0.00124(4)	0.000014(1)	0.0878(2)	
1163.110746(7)	9	2	A1	9	3	A2	^{P}Q(9,3,A2)	35.93(5)	0.0639(1)	0.0586	0.778(2)	0.655(2)	−0.00124(4)	0.000014(1)	0.0878(2)	
1163.474647(54)	2	1	A1	1	0	A2	^{R}R(1,0,A2)	0.56(0)	0.0768(15)							
1163.714357(8)	8	2	A1	8	3	A2	^{P}Q(8,3,A2)	43.63(3)	0.0645(1)	0.0595	0.826(2)	0.663(3)	−0.00212(4)	0.000026(1)	0.0869(1)	
1163.787924(8)	8	2	A2	8	3	A1	^{P}Q(8,3,A1)	42.83(4)	0.0645(1)	0.0595	0.826(2)	0.663(3)	−0.00212(4)	0.000026(1)	0.0869(1)	
1163.913919(7)	1	1	A2	0	0	A1	^{R}R(0,0,A1)	35.40(2)	0.0646(1)		0.786(2)		−0.00096(8)	0.000007(1)	0.0913(14)	0.749(33)
1164.049765(15)	12	3	E	12	4	E	^{P}Q(12,4,E)	14.48(4)	0.0559(2)	0.0553		0.621(1)	−0.00255(16)		0.0768(16)	

Table 5 (*continued*)

Position, cm^{-1}	J′	K′	S′	J″	K″	S″	Assignment	Int*10[25a]	$b_L^0(N_2)$ expt,[b]	$b_L^0(N_2)$ calc.[b]	n_1 expt	n_1 calc.	$\delta^0(N_2)$ expt[b]	$\delta'(N_2)$ expt[c]	$b_L^0(self)$ expt[b]	n_2 expt
1164.381569(5)	7	2	A2	7	3	A1	^{P}Q(7,3,A1)	48.71(4)	0.0672(1)	0.0607	0.828(2)	0.672(4)	−0.00239(3)	0.000024(2)	0.0876(4)	0.750(13)
1164.426483(5)	7	2	A1	7	3	A2	^{P}Q(7,3,A2)	47.97(5)	0.0672(1)	0.0607	0.828(2)	0.672(4)	−0.00239(3)	0.000024(2)	0.0876(4)	
1164.934109(10)	11	3	E	11	4	E	^{P}Q(11,4,E)	19.32(4)	0.0553(2)	0.0559	0.902(15)	0.628(1)			0.0955(33)	0.41(37)
1164.989362(4)	6	2	A1	6	3	A2	^{P}Q(6,3,A2)	50.48(1)	0.0696(1)	0.0621	0.843(2)	0.685(5)	−0.00232(3)	0.000025(2)	0.0906(1)	0.715(1)
1165.014728(4)	6	2	A2	6	3	A1	^{P}Q(6,3,A1)	50.48(1)	0.0696(1)	0.0621	0.843(2)	0.685(5)	−0.00232(3)	0.000025(2)	0.0906(1)	0.715(1)
1165.528810(6)	5	2	A2	5	3	A1	^{P}Q(5,3,A1)	48.03(1)	0.0641(0)	0.0639	0.845(1)	0.703(6)	−0.00205(4)	0.000015(2)	0.0896(2)	
1165.541406(6)	5	2	A1	5	3	A2	^{P}Q(5,3,A2)	48.03(1)	0.0641(0)	0.0639	0.845(1)	0.703(6)	−0.00205(4)	0.000015(2)	0.0896(2)	
1165.788102(8)	10	3	E	10	4	E	^{P}Q(10,4,E)	25.47(4)	0.0570(1)	0.0566	0.737(7)	0.635(1)	−0.00289(11)	0.000026(2)	0.0788(5)	
1165.991512(12)	4	2	A1	4	3	A2	^{P}Q(4,3,A2)	40.25(1)	0.0667(0)	0.0660	0.853(0)	0.728(6)	−0.00141(4)	0.000010(2)	0.0891(2)	
1165.996906(12)	4	2	A2	4	3	A1	^{P}Q(4,3,A1)	40.25(1)	0.0667(0)	0.0660	0.853(0)	0.728(6)	−0.00141(4)	0.000010(2)	0.0891(2)	
1166.370334(12)	3	2	A2	3	3	A1	^{P}Q(3,3,A1)	25.32(1)	0.0703(1)	0.0678	0.864(1)	0.751(7)		0.000005(2)	0.0927(2)	
1166.508093(33)	13	4	E	13	5	E	^{P}Q(13,5,E)	8.56(6)	0.0536(3)	0.0539		0.609(1)			0.0711(36)	
1166.602608(7)	9	3	E	9	4	E	^{P}Q(9,4,E)	30.78(4)	0.0566(1)	0.0575	0.796(5)	0.642(2)	−0.00242(9)	0.000026(2)	0.0824(4)	
1167.368139(6)	8	3	E	8	4	E	^{P}Q(8,4,E)	36.36(3)	0.0586(1)	0.0586	0.799(3)	0.652(3)	−0.00315(7)	0.000012(1)	0.0820(2)	
1167.522215(12)	12	4	E	12	5	E	^{P}Q(12,5,E)	12.37(2)	0.0535(2)	0.0544	0.695(17)	0.614(1)	−0.00321(16)			
1168.075586(6)	7	3	E	7	4	E	^{P}Q(7,4,E)	39.93(3)	0.0613(1)	0.0602	0.796(3)	0.667(4)	−0.00246(7)	0.000018(1)		
1168.270282(5)	2	2	E	1	1	E	^{R}R(1,1,E)	51.87(2)	0.0654(1)	0.0684	0.844(1)	0.757(6)	−0.00139(5)		0.0881(0)	
1168.500905(9)	11	4	E	11	5	E	^{P}Q(11,5,E)	16.89(2)	0.0549(1)	0.0550	0.709(11)	0.620(1)	−0.00322(13)	0.000021(3)		
1168.715933(5)	6	3	E	6	4	E	^{P}Q(6,4,E)	39.82(2)	0.0639(1)	0.0624	0.828(2)	0.692(6)	−0.00242(7)			
1168.909810(22)	14	5	A1	14	6	A2	^{P}Q(14,6,A2)	9.98(2)	0.0517(2)	0.0528	0.512(28)	0.601(2)	−0.00303(19)		0.0688(30)	
1169.280994(5)	5	3	E	5	4	E	^{P}Q(5,4,E)	34.79(2)	0.0671(1)	0.0648	0.849(2)	0.722(6)	−0.00152(8)		0.0880(2)	
1169.435777(7)	10	4	E	10	5	E	^{P}Q(10,5,E)	21.72(3)	0.0556(1)	0.0559	0.733(8)	0.628(1)	−0.00389(11)			
1169.763499(6)	4	3	E	4	4	E	^{P}Q(4,4,E)	22.23(2)	0.0700(1)	0.0668	0.861(2)	0.747(7)	−0.00187(11)		0.0931(2)	
1170.060167(13)	13	5	A2	13	6	A1	^{P}Q(13,6,A1)	14.88(2)	0.0514(2)	0.0532	0.686(16)	0.605(1)	−0.00345(13)			
1170.318393(6)	9	4	E	9	5	E	^{P}Q(9,5,E)	26.23(2)	0.0566(1)	0.0572	0.772(5)	0.639(1)	−0.00334(8)	0.000014(2)		
1171.140276(6)	8	4	E	8	5	E	^{P}Q(8,5,E)	29.90(4)	0.0593(1)	0.0590	0.774(5)	0.659(3)	−0.00279(12)	0.000020(2)	0.0820(3)	
1171.170415(11)	12	5	A1	12	6	A2	^{P}Q(12,6,A2)	21.32(5)	0.0512(2)	0.0539	0.754(16)	0.611(1)	−0.00337(14)		0.0721(10)	
1171.352383(5)	2	1	A1	1	0	A2	^{R}R(1,0,A2)	52.75(2)	0.0659(0)	0.0709	0.843(1)	0.763(6)	−0.00072(5)	0.000004(1)	0.0903(1)	
1171.893414(6)	7	4	E	7	5	E	^{P}Q(7,5,E)	30.81(2)	0.0614(1)	0.0614	0.822(3)	0.687(5)	−0.00197(8)	0.000012(1)	0.0847(2)	
1172.232987(7)	11	5	A1	11	6	A2	^{P}Q(11,6,A2)	28.2(3)	0.0524(1)	0.0549	0.720(7)	0.619(1)	−0.00364(7)	0.000020(2)		
1172.570194(6)	6	4	E	6	5	E	^{P}Q(6,5,E)	27.99(5)	0.0655(2)	0.0640	0.858(7)	0.718(6)	−0.00196(15)	0.000020(2)	0.0870(3)	
1172.601008(5)	3	3	E	2	2	E	^{R}R(2,2,E)	77.51(4)	0.0653(1)	0.0663	0.851(1)	0.744(6)	−0.00111(6)	0.000004(2)	0.0874(1)	
1173.163727(6)	5	4	E	5	5	E	^{P}Q(5,5,E)	18.56(3)	0.0695(2)	0.0657	0.854(3)	0.742(7)			0.0907(3)	
1173.240002(6)	10	5	A1	10	6	A2	^{P}Q(10,6,A2)	35.79(4)	0.0544(1)	0.0563	0.750(5)	0.633(1)	−0.00318(7)	0.000016(1)	0.0768(3)	
1173.771460(25)	13	6	E	13	7	E	^{P}Q(13,7,E)	6.35(2)	0.0500(3)	0.0532	0.647(37)	0.605(1)	−0.00477(31)		0.0601(32)	
1174.183837(6)	9	5	A1	9	6	A2	^{P}Q(9,6,A2)	42.51(3)	0.0570(1)	0.0584	0.754(4)	0.655(2)	−0.00303(6)	0.000014(1)		
1174.973264(42)	12	6	E	12	7	E	^{P}Q(12,7,E)	8.89(3)	0.0505(4)	0.0543	0.587(35)	0.614(1)	−0.00560(45)	0.000068(8)	0.0594(32)	
1174.978732(18)	2	0	E	1	1	E	^{P}R(1,1,E)	7.98(2)	0.0671(5)	0.0710	0.843(7)	0.764(6)			0.0952(9)	
1175.743244(6)	3	2	E	2	1	E	^{R}R(2,1,E)	57.05(2)	0.0634(1)	0.0679	0.836(1)	0.743(6)	−0.00086(5)	0.000009(2)	0.0835(8)	0.784(23)
1175.852436(6)	7	5	A1	7	6	A2	^{P}Q(7,6,A2)	42.70(3)	0.0638(1)	0.0633	0.817(3)	0.712(6)	−0.00102(6)		0.0852(2)	
1176.115511(13)	11	6	E	11	7	E	^{P}Q(11,7,E)	11.51(2)	0.0514(2)	0.0559	0.744(17)	0.629(1)	−0.00429(16)		0.0748(16)	
1176.563597(6)	6	5	A1	6	6	A2	^{P}Q(6,6,A2)	28.76(2)	0.0666(1)	0.0647	0.858(3)	0.735(7)			0.0893(3)	
1176.974032(5)	4	4	A1	3	3	A2	^{R}R(3,3,A2)	186.38(3)	0.0630(0)	0.0647	0.822(1)	0.734(6)	−0.00108(3)	0.000004(2)	0.0814(4)	0.801(11)
1177.191505(10)	10	6	E	10	7	E	^{P}Q(10,7,E)	14.55(2)	0.0556(2)	0.0580	0.692(12)	0.650(2)	−0.00307(14)		0.0768(10)	
1178.194155(9)	9	6	E	9	7	E	^{P}Q(9,7,E)	16.24(2)	0.0598(2)	0.0603	0.742(9)	0.677(3)	−0.00225(13)		0.0798(7)	
1178.629294(6)	3	1	A2	2	0	A1	^{R}R(2,0,A1)	67.23(2)	0.0667(0)	0.0695	0.845(1)	0.748(6)	−0.00159(4)	0.000010(2)	0.0889(2)	
1178.921575(23)	12	7	E	12	8	E	^{P}Q(12,8,E)	7.19(2)	0.0498(3)	0.0556		0.624(1)	−0.00413(22)		0.0683(28)	
1179.116925(8)	8	6	E	8	7	E	^{P}Q(8,7,E)	15.21(2)	0.0608(2)	0.0626	0.801(8)	0.705(5)			0.0878(7)	
1179.953709(9)	7	6	E	7	7	E	^{P}Q(7,7,E)	11.28(3)	0.0648(3)	0.0638	0.858(9)	0.728(6)		0.000047(7)	0.0759(9)	

1179.987401(6)	4	3	E	3	2	E	^{R}R(3,2,E)	76.03(3)	0.0651(1)	0.0663	0.846(1)	0.733(6)	−0.00093(5)	0.000013(1)	0.0860(2)	0.750(0)
1180.144243(23)	11	7	E	11	8	E	^{P}Q(11,8,E)	9.31(4)	0.0497(2)	0.0576	0.757(23)	0.644(1)	−0.00239(20)			
1181.390665(5)	5	5	E	4	4	E	^{R}R(4,4,E)	97.66(2)	0.0587(0)	0.0632	0.801(1)	0.723(6)	−0.00126(3)	0.000007(2)	0.0763(5)	0.843(16)
1182.350649(11)	9	7	E	9	8	E	^{P}Q(9,8,E)	10.25(3)	0.0590(2)	0.0619		0.695(4)			0.0631(13)	
1182.476326(7)	3	0	E	2	1	E	^{P}R(2,1,E)	14.04(2)	0.0677(2)	0.0695	0.854(3)	0.749(6)		0.000012(2)	0.0906(3)	
1183.014330(15)	12	8	A1	12	9	A2	^{P}Q(12,9,A2)	11.22(2)	0.0511(2)	0.0572		0.637(1)	−0.00246(15)		0.0670(19)	
1183.099278(6)	4	2	E	3	1	E	^{R}R(3,1,E)	61.95(2)	0.0635(0)	0.0666	0.835(1)	0.725(6)	−0.00065(5)	0.000008(1)	0.0820(2)	0.840(16)
1183.323054(12)	8	7	E	8	8	E	^{P}Q(8,8,E)	7.71(1)	0.0645(3)	0.0628	0.879(16)	0.718(6)	0.00416(23)		0.0833(14)	
1184.273226(5)	5	4	A1	4	3	A2	^{R}R(4,3,A2)	170.58(3)	0.0648(0)	0.0653	0.836(1)	0.727(6)	−0.00102(3)	0.000008(2)	0.0826(3)	0.846(9)
1184.320459(12)	11	8	A1	11	9	A2	^{P}Q(11,9,A2)	13.97(3)	0.0544(2)	0.0592		0.659(2)			0.0681(15)	
1185.536801(10)	10	8	A1	10	9	A2	^{P}Q(10,9,A2)	13.87(2)	0.0583(2)	0.0611		0.684(4)			0.0787(12)	
1185.744718(6)	4	1	A1	3	0	A2	^{R}R(3,0,A2)	76.92(3)	0.0668(0)	0.0679	0.847(1)	0.734(6)	−0.00111(4)	0.000006(1)	0.0883(2)	
1185.851958(5)	6	6	E	5	5	E	^{R}R(5,5,E)	92.39(3)	0.0542(0)	0.0620	0.751(1)	0.712(5)	−0.00157(3)	0.000006(2)	0.0745(1)	
1185.990482(10)	3	1	E	2	2	E	^{P}R(2,2,E)	5.17(1)	0.0704(4)	0.0691	0.871(10)	0.753(7)	−0.00427(40)		0.0906(9)	
1186.658408(11)	9	8	A1	9	9	A2	^{P}Q(9,9,A2)	10.61(2)	0.0632(2)	0.0618		0.707(5)	0.00507(17)		0.0786(12)	
1187.263042(11)	5	3	E	4	2	E	^{R}R(4,2,E)	73.60(2)	0.0634(1)	0.0644	0.843(1)	0.706(6)	−0.00091(6)	0.000009(1)	0.0806(2)	
1188.602551(5)	6	5	E	5	4	E	^{R}R(5,4,E)	85.56(2)	0.0635(0)	0.0645	0.816(1)	0.721(6)	−0.00158(4)	0.000006(2)	0.0827(2)	
1189.904653(6)	4	0	E	3	1	E	^{P}R(3,1,E)	16.88(1)	0.0670(1)	0.0679	0.843(2)	0.736(6)	−0.00180(14)		0.0898(3)	
1190.322385(7)	5	2	E	4	1	E	^{R}R(4,1,E)	65.66(5)	0.0631(1)	0.0651	0.832(1)	0.711(6)	−0.00080(7)	0.000009(1)	0.0848(16)	0.718(42)
1190.358540(6)	7	7	A1	6	6	A2	^{R}R(6,6,A2)	162.96(8)	0.0507(1)	0.0607	0.706(1)	0.699(4)	−0.00141(3)	0.000008(2)	0.0689(4)	0.693(13)
1191.463969(5)	6	4	A1	5	3	A2	^{R}R(5,3,A2)	154.91(3)	0.0635(0)	0.0630	0.826(1)	0.697(5)	−0.00108(3)	0.000009(2)	0.0901(4)	0.581(11)
1192.699138(6)	5	1	A2	4	0	A1	^{R}R(4,0,A1)	81.58(2)	0.0660(0)	0.0663	0.847(1)	0.722(6)	−0.00113(4)	0.000009(2)	0.0881(1)	
1192.976955(6)	7	6	E	6	5	E	^{R}R(6,5,E)	77.01(3)	0.0606(0)	0.0636	0.793(1)	0.713(6)	−0.00160(4)	0.000012(2)	0.0815(2)	
1193.384516(7)	4	1	E	3	2	E	^{P}R(3,2,E)	9.66(1)	0.0664(2)	0.0670	0.854(3)	0.733(6)			0.0896(5)	
1194.417528(6)	6	3	E	5	2	E	^{R}R(5,2,E)	69.73(2)	0.0622(0)	0.0626	0.818(1)	0.685(5)	−0.00076(4)	0.000007(2)	0.0821(1)	
1194.910923(5)	8	8	E	7	7	E	^{R}R(7,7,E)	65.71(2)	0.0444(0)	0.0596	0.646(2)	0.685(3)	−0.00146(3)	0.000008(2)	0.0630(1)	
1195.706526(6)	7	5	E	6	4	E	^{R}R(6,4,E)	72.99(3)	0.0624(0)	0.0622	0.810(1)	0.692(5)	−0.00154(4)	0.000010(2)	0.0818(2)	
1197.278810(7)	5	0	E	4	1	E	^{P}R(4,1,E)	17.21(2)	0.0667(1)	0.0663	0.828(2)	0.722(6)			0.0896(3)	
1197.396019(22)	6	2	E	5	1	E	^{R}R(5,1,E)	66.96(8)	0.0699(3)	0.0637	0.761(4)	0.700(6)		0.000013(2)	0.0799(23)	
1197.396721(18)	8	7	A1	7	6	A2	^{R}R(7,6,A2)	129.39(10)	0.0556(1)	0.0627	0.751(3)	0.703(5)	−0.00224(14)	0.000007(1)	0.0800(18)	
1198.536940(9)	7	4	A2	6	3	A1	^{R}R(6,3,A1)	67.72(1)	0.0618(0)	0.0607	0.797(1)	0.668(4)	−0.00121(2)		0.0746(1)	0.948(2)
1198.542387(15)	7	4	A1	6	3	A2	^{R}R(6,3,A2)	67.72(1)	0.0618(0)	0.0607	0.797(1)	0.668(4)	−0.00121(2)		0.0746(1)	0.948(2)
1199.493392(8)	6	1	A1	5	0	A2	^{R}R(5,0,A2)	80.71(4)	0.0665(1)	0.0647	0.818(2)	0.711(6)	−0.00120(7)		0.0841(2)	
1199.509368(8)	9	9	E	8	8	E	^{R}R(8,8,E)	49.69(7)	0.0394(1)	0.0585	0.585(5)	0.669(2)	−0.00206(7)	0.000011(1)		
1199.994381(6)	8	6	E	7	5	E	^{R}R(7,5,E)	62.68(3)	0.0599(1)	0.0616	0.797(2)	0.688(5)	−0.00175(5)	0.000011(1)	0.0822(2)	
1200.701589(7)	5	1	E	4	2	E	^{P}R(4,2,E)	12.71(1)	0.0656(2)	0.0654	0.839(4)	0.716(6)		0.000016(2)		
1201.439678(6)	7	3	E	6	2	E	^{R}R(6,2,E)	63.68(2)	0.0609(1)	0.0611	0.803(1)	0.672(4)	−0.00090(4)	0.000004(1)	0.0814(2)	
1201.862535(6)	9	8	E	8	7	E	^{R}R(8,7,E)	50.14(3)	0.0544(1)	0.0618	0.749(3)	0.691(4)	−0.00180(5)	0.000018(1)		
1202.695902(6)	8	5	E	7	4	E	^{R}R(7,4,E)	60.73(3)	0.0602(1)	0.0597	0.799(2)	0.661(3)	−0.00111(5)	0.000010(1)	0.0799(2)	
1204.304894(16)	7	2	E	6	1	E	^{R}R(6,1,E)	63.93(11)	0.0640(1)	0.0624	0.871(3)	0.690(5)	−0.00143(11)	0.000015(1)	0.0837(4)	
1204.327733(7)	9	7	A1	8	6	A2	^{R}R(8,6,A2)	100.34(10)	0.0579(1)	0.0610	0.777(3)	0.680(3)	−0.00212(6)	0.000026(1)	0.0791(2)	
1204.614848(7)	6	0	E	5	1	E	^{P}R(5,1,E)	15.14(2)	0.0662(2)	0.0647	0.822(4)	0.711(6)	−0.00149(11)		0.0877(4)	
1205.485111(8)	8	4	A1	7	3	A2	^{R}R(7,3,A2)	57.72(3)	0.0655(1)	0.0590	0.794(2)	0.649(3)	−0.00140(3)		0.0854(1)	
1205.529251(8)	8	4	A2	7	3	A1	^{R}R(7,3,A1)	48.93(4)	0.0655(1)	0.0590	0.794(2)	0.649(3)	−0.00140(3)		0.0854(1)	
1206.128962(6)	7	1	A2	6	0	A1	^{R}R(6,0,A1)	75.67(2)	0.0653(0)	0.0633	0.829(1)	0.700(6)	−0.00191(4)	0.000009(1)	0.0845(2)	
1206.374111(7)	10	9	E	9	8	E	^{R}R(9,8,E)	36.01(4)	0.0508(1)	0.0609	0.706(5)	0.675(3)	−0.00266(8)	0.000010(1)	0.0746(3)	
1206.898332(6)	9	6	E	8	5	E	^{R}R(8,5,E)	49.45(3)	0.0578(1)	0.0591	0.778(2)	0.658(2)	−0.00190(5)	0.000009(1)		
1207.951494(7)	6	1	E	5	2	E	^{P}R(5,2,E)	13.50(2)	0.0636(2)	0.0639	0.830(4)	0.703(6)	−0.00221(16)	0.000021(2)		
1208.318059(6)	8	3	E	7	2	E	^{R}R(7,2,E)	56.01(2)	0.0599(1)	0.0599	0.796(2)	0.664(4)	−0.00111(5)			
1208.706761(6)	10	8	E	9	7	E	^{R}R(9,7,E)	37.57(3)	0.0557(1)	0.0604	0.744(4)	0.669(2)	−0.00141(6)	0.000015(1)	0.0766(3)	
1208.844713(8)	11	11	E	10	10	E	^{R}R(10,10,E)	23.03(2)	0.0306(1)	0.0564	0.445(7)	0.639(1)	−0.00237(5)	0.000012(1)		
1209.563871(6)	9	5	E	8	4	E	^{R}R(8,4,E)	48.62(3)	0.0580(1)	0.0576	0.773(2)	0.638(1)	−0.00125(5)			
1210.931527(6)	11	10	A1	10	9	A2	^{R}R(10,9,A2)	49.31(4)	0.0479(1)	0.0599	0.677(5)	0.659(1)	−0.00241(5)	0.000019(1)	0.0704(3)	
1211.037407(6)	8	2	E	7	1	E	^{R}R(7,1,E)	58.58(4)	0.0631(1)	0.0612	0.817(2)	0.681(5)	−0.00140(6)	0.000008(1)	0.0828(2)	

Table 5 (*continued*)

Position, cm^{-1}	J′	K′	S′	J″	K″	S″	Assignment	Int*10[25a]	$b_L^0(N_2)$ expt,[b]	$b_L^0(N_2)$ calc.[b]	n_1 expt	n_1 calc.	$\delta^0(N_2)$ expt[b]	$\delta'(N_2)$ expt[c]	$b_L^0(self)$ expt[b]	n_2 expt
1211.145943(6)	10	7	A1	9	6	A2	^{R}R(9,6,A2)	75.55(4)	0.0559(1)	0.0586	0.747(2)	0.653(2)	−0.00200(4)	0.000012(1)	0.0781(2)	
1211.492823(9)	6	2	A1	5	3	A2	^{P}R(5,3,A2)	8.88(1)	0.0635(1)	0.0632	0.843(1)	0.697(6)	−0.00185(9)	0.000018(1)	0.0953(4)	
1211.517931(9)	6	2	A2	5	3	A1	^{P}R(5,3,A1)	8.96(1)	0.0635(1)	0.0632	0.843(1)	0.697(6)	−0.00185(9)	0.000018(1)	0.0953(4)	
1211.927987(8)	7	0	E	6	1	E	^{P}R(6,1,E)	11.90(2)	0.0652(3)	0.0633	0.822(5)	0.700(6)			0.0892(6)	
1212.252462(6)	9	4	A1	8	3	A2	^{R}R(8,3,A2)	46.20(3)	0.0642(1)	0.0577	0.809(2)	0.639(2)	−0.00123(3)	0.000003(2)	0.0853(1)	
1212.298834(8)	9	4	A2	8	3	A1	^{R}R(8,3,A1)	47.57(4)	0.0642(1)	0.0577	0.809(2)	0.639(2)	−0.00123(3)	0.000003(2)	0.0853(1)	
1212.607277(6)	8	1	A1	7	0	A2	^{R}R(7,0,A2)	66.81(3)	0.0644(1)	0.0620	0.824(1)	0.690(5)	−0.00221(5)	0.000018(1)	0.0852(2)	
1213.131507(8)	11	9	E	10	8	E	^{R}R(10,8,E)	25.65(3)	0.0519(1)	0.0596	0.708(7)	0.656(1)	−0.00251(9)		0.0814(6)	
1213.581159(12)	12	12	E	11	11	E	^{R}R(11,11,E)	14.96(2)	0.0277(1)	0.0554	0.36(14)	0.627(1)	−0.00187(8)	0.000021(2)	0.0434(12)	
1213.682846(7)	10	6	E	9	5	E	^{R}R(9,5,E)	37.66(5)	0.0562(1)	0.0568	0.721(6)	0.633(1)	−0.00148(14)		0.0778(3)	
1215.042024(6)	9	3	E	8	2	E	^{R}R(8,2,E)	47.34(3)	0.0597(1)	0.0589	0.783(2)	0.656(3)	−0.00134(6)	0.000006(1)	0.0806(2)	
1215.145227(8)	7	1	E	6	2	E	^{P}R(6,2,E)	12.92(2)	0.0637(2)	0.0625	0.811(5)	0.692(5)	−0.0033(21)		0.0863(5)	
1215.208733(12)	6	3	E	5	4	E	^{P}R(5,4,E)	4.75(1)	0.0679(5)	0.0643	0.893(11)	0.719(7)			0.0916(14)	
1215.438903(7)	11	8	E	10	7	E	^{R}R(10,7,E)	26.76(3)	0.0529(1)	0.0582	0.728(7)	0.645(1)	−0.00195(9)		0.0777(5)	
1215.534491(11)	12	11	E	11	10	E	^{R}R(11,10,E)	16.08(3)	0.0451(2)	0.0588	0.627(14)	0.644(1)	−0.00389(12)	0.000027(3)	0.0722(13)	
1216.303890(6)	10	5	E	9	4	E	^{R}R(9,4,E)	37.61(3)	0.0561(1)	0.0561	0.765(4)	0.624(1)	−0.00146(7)		0.0771(3)	
1217.588040(11)	9	2	E	8	1	E	^{R}R(8,1,E)	50.40(5)	0.0626(1)	0.0602	0.803(4)	0.671(3)		0.000015(2)	0.0831(4)	
1217.601718(14)	12	10	A1	11	9	A2	^{R}R(11,9,A2)	33.76(7)	0.0499(2)	0.0588	0.669(13)	0.643(1)	−0.00339(17)	0.000021(3)	0.077(12)	
1217.846109(6)	11	7	A1	10	6	A2	^{R}R(10,6,A2)	55.02(3)	0.0532(1)	0.0564	0.728(3)	0.629(1)	−0.00208(5)	0.000011(1)	0.0765(2)	
1218.362994(12)	13	13	A1	12	12	A2	^{R}R(12,12,A2)	17.17(2)	0.0239(1)	0.0545	0.264(14)	0.616(1)	−0.00236(6)	0.000016(1)	0.0481(15)	
1218.616479(8)	7	2	A2	6	3	A1	^{P}R(6,3,A1)	9.94(1)	0.0674(2)	0.0615	0.872(5)	0.679(5)	−0.00206(7)	0.000012(1)	0.0889(3)	
1218.661262(9)	7	2	A1	6	3	A2	^{P}R(6,3,A2)	9.91(2)	0.0674(2)	0.0615	0.872(5)	0.679(5)	−0.00206(7)	0.000012(1)	0.0889(3)	
1218.930369(9)	9	1	A2	8	0	A1	^{R}R(8,0,A1)	55.98(11)	0.0620(1)	0.0608	0.797(3)	0.678(4)			0.0843(5)	
1218.933810(9)	10	4	A2	9	3	A1	^{R}R(9,3,A1)	37.28(4)	0.0641(0)	0.0568	0.809(0)	0.633(1)	−0.00201(4)		0.0865(3)	
1218.969303(6)	10	4	A1	9	3	A2	^{R}R(9,3,A2)	37.28(4)	0.0641(0)	0.0568	0.809(0)	0.633(1)	−0.00201(4)		0.0865(3)	
1219.229417(9)	8	0	E	7	1	E	^{P}R(7,1,E)	8.64(2)	0.0640(3)	0.0620	0.850(8)	0.690(5)		0.000034(4)	0.0857(9)	
1219.777253(10)	12	9	E	11	8	E	^{R}R(11,8,E)	17.98(3)	0.0507(2)	0.0577	0.677(11)	0.635(1)	−0.00148(12)	0.000018(2)	0.0806(11)	
1220.342003(7)	11	6	E	10	5	E	^{R}R(10,5,E)	27.91(3)	0.0541(1)	0.0551	0.735(6)	0.616(1)	−0.00117(8)	0.000011(2)	0.0768(4)	
1221.602529(6)	10	3	E	9	2	E	^{R}R(9,2,E)	38.94(3)	0.0601(1)	0.0581	0.769(3)	0.648(2)	−0.00172(6)	0.000007(1)	0.0757(3)	
1222.054179(9)	12	8	E	11	7	E	^{R}R(11,7,E)	18.98(3)	0.0509(1)	0.0561	0.694(10)	0.623(1)	−0.00125(10)	0.000018(2)	0.0708(9)	
1222.911308(7)	11	5	E	10	4	E	^{R}R(10,4,E)	27.98(3)	0.0546(1)	0.0551	0.777(5)	0.616(1)	−0.00124(7)		0.0752(4)	
1223.189452(68)	14	14	E	13	13	E	^{R}R(13,13,E)	4.61(5)	0.0209(3)	0.0537	0.580(53)	0.608(1)	−0.00397(19)		0.0537(10)	
1223.955802(6)	10	2	E	9	1	E	^{R}R(9,1,E)	41.50(3)	0.0621(1)	0.0592	0.811(3)	0.660(2)	−0.00188(6)	0.000010(1)	0.0795(3)	
1224.160571(10)	13	10	A1	12	9	A2	^{R}R(12,9,A2)	22.36(3)	0.0479(1)	0.0571	0.653(11)	0.625(1)	−0.00276(8)		0.0723(22)	0.834(72)
1224.423081(7)	12	7	A1	11	6	A2	^{R}R(11,6,A2)	38.64(3)	0.0512(1)	0.0546	0.728(5)	0.612(1)	−0.00221(5)	0.000009(1)	0.0713(4)	
1225.100230(6)	10	1	A1	9	0	A2	^{R}R(9,0,A2)	45.07(3)	0.0633(1)	0.0598	0.803(3)	0.665(3)	−0.00134(6)	0.000008(1)	0.0785(9)	0.819(27)
1225.452547(7)	11	4	A1	10	3	A2	^{R}R(10,3,A2)	28.71(3)	0.0620(1)	0.0561	0.752(6)	0.627(1)	−0.00227(4)	0.000016(1)	0.0825(2)	
1225.488360(7)	11	4	A2	10	3	A1	^{R}R(10,3,A1)	28.59(3)	0.0620(1)	0.0561	0.752(6)	0.627(1)	−0.00227(4)	0.000016(1)	0.0825(2)	
1225.671923(9)	8	2	A1	7	3	A2	^{P}R(7,3,A2)	9.24(1)	0.0656(1)	0.0601	0.829(5)	0.668(4)	−0.00318(7)	0.000018(1)	0.0891(4)	
1225.745502(9)	8	2	A2	7	3	A1	^{P}R(7,3,A1)	9.14(2)	0.0656(1)	0.0601	0.829(5)	0.668(4)	−0.00318(7)	0.000018(1)	0.0891(4)	
1226.100182(17)	7	4	E	6	5	E	^{P}R(6,5,E)	3.15(1)	0.0666(6)	0.0636	0.868(19)	0.718(7)			0.0868(20)	
1226.307017(14)	13	9	E	12	8	E	^{R}R(12,8,E)	11.90(2)	0.0484(2)	0.0558	0.674(18)	0.617(1)	−0.00196(13)		0.0673(19)	
1226.525196(13)	9	0	E	8	1	E	^{P}R(8,1,E)	5.71(1)	0.0628(4)	0.0609	0.831(14)	0.679(4)			0.0815(15)	
1226.870391(9)	12	6	E	11	5	E	^{R}R(11,5,E)	20.02(3)	0.0530(1)	0.0540	0.761(9)	0.607(1)	−0.00181(9)		0.0740(8)	
1227.993000(7)	11	3	E	10	2	E	^{R}R(10,2,E)	29.66(3)	0.0584(1)	0.0573	0.796(5)	0.639(1)	−0.00161(9)		0.0805(4)	
1228.547887(14)	13	8	E	12	7	E	^{R}R(12,7,E)	12.65(2)	0.0478(2)	0.0543	0.727(20)	0.607(1)	−0.00209(17)		0.0748(18)	
1229.311759(11)	8	3	E	7	4	E	^{P}R(7,4,E)	6.71(1)	0.0605(3)	0.0596	0.845(12)	0.662(4)	−0.00391(36)		0.0859(12)	
1229.389521(10)	12	5	E	11	4	E	^{R}R(11,4,E)	19.74(3)	0.0544(2)	0.0544	0.736(17)	0.611(1)			0.0788(11)	
1229.409797(11)	9	1	E	8	2	E	^{P}R(8,2,E)	8.56(2)	0.0624(5)	0.0602	0.837(16)	0.672(4)			0.0827(14)	

1230.143728(7)	11	2	E	10	1	E	^{R}R(10,1,E)	31.50(3)	0.0603(1)	0.0582	0.786(5)	0.648(1)	−0.00224(9)	0.000021(2)	0.0836(4)
1230.604297(15)	14	10	A1	13	9	A2	^{R}R(13,9,A2)	14.64(3)	0.0464(2)	0.0554		0.609(1)			
1230.871883(9)	13	7	A1	12	6	A2	^{R}R(12,6,A2)	26.33(3)	0.0502(1)	0.0534	0.634(10)	0.601(2)	−0.00228(9)	0.000025(2)	
1231.119627(7)	11	1	A2	10	0	A1	^{R}R(10,0,A1)	34.11(3)	0.0621(1)	0.0587	0.789(5)	0.652(1)	−0.00162(8)	0.000021(2)	0.0841(4)
1231.811182(9)	12	4	A2	11	3	A1	^{R}R(11,3,A1)	20.94(3)	0.0606(1)	0.0555	0.813(9)	0.621(1)	−0.00142(5)	0.000021(1)	0.0850(3)
1231.848733(9)	12	4	A1	11	3	A2	^{R}R(11,3,A2)	20.92(3)	0.0606(1)	0.0555	0.813(9)	0.621(1)	−0.00142(5)	0.000021(1)	0.0850(3)
1232.667550(11)	9	2	A2	8	3	A1	^{P}R(8,3,A1)	7.95(1)	0.0626(2)	0.0591	0.841(5)	0.659(3)	−0.00227(12)	0.000023(3)	0.0882(9)
1232.781012(11)	9	2	A1	8	3	A2	^{P}R(8,3,A2)	7.98(1)	0.0626(2)	0.0591	0.841(5)	0.659(3)	−0.00227(12)	0.000023(3)	0.0882(9)
1233.060408(72)	15	12	E	14	11	E	^{R}R(14,11,E)	3.80(3)	0.0431(5)	0.0559		0.606(1)	−0.00415(36)		
1233.263806(13)	13	6	E	12	5	E	^{R}R(12,5,E)	13.92(2)	0.0528(2)	0.0533	0.652(18)	0.601(2)	−0.00184(16)		
1234.209695(8)	12	3	E	11	2	E	^{R}R(11,2,E)	21.97(3)	0.0580(1)	0.0565	0.747(8)	0.630(1)	−0.00224(11)		0.0810(7)
1234.915629(22)	14	8	E	13	7	E	^{R}R(13,7,E)	8.20(2)	0.0466(3)	0.0530	0.579(31)	0.597(2)			0.0637(30)
1235.820952(15)	13	5	E	12	4	E	^{R}R(12,4,E)	10.34(2)	0.0568(3)	0.0539	0.717(21)	0.607(1)	−0.00145(11)		0.0776(19)
1236.157291(8)	12	2	E	11	1	E	^{R}R(11,1,E)	23.41(4)	0.0598(2)	0.0574	0.753(10)	0.636(1)	−0.00228(12)	0.000024(3)	0.0849(7)
1236.257241(13)	9	3	E	8	4	E	^{P}R(8,4,E)	6.25(1)	0.0598(4)	0.0581	0.795(16)	0.647(2)	−0.00328(20)	0.000054(6)	0.0815(15)
1236.501073(15)	10	1	E	9	2	E	^{P}R(9,2,E)	6.03(1)	0.0621(4)	0.0592	0.798(19)	0.661(2)			0.0839(17)
1236.960540(17)	8	5	A1	7	6	A2	^{P}R(7,6,A2)	4.13(1)	0.0672(7)	0.0631		0.716(6)			0.0858(20)
1236.991242(8)	12	1	A1	11	0	A2	^{R}R(11,0,A2)	24.53(4)	0.0608(2)	0.0578	0.801(11)	0.640(1)	−0.00197(14)		0.0879(7)
1237.188272(13)	14	7	A1	13	6	A2	^{R}R(13,6,A2)	17.18(3)	0.0494(2)	0.0525	0.710(16)	0.595(2)	−0.00223(12)		0.0724(16)
1238.006728(12)	13	4	A1	12	3	A2	^{R}R(12,3,A2)	14.92(2)	0.0599(2)	0.0549	0.803(16)	0.614(1)	−0.00191(6)	0.000015(1)	0.0869(6)
1238.044758(12)	13	4	A2	12	3	A1	^{R}R(12,3,A1)	14.76(2)	0.0599(2)	0.0549	0.803(16)	0.614(1)	−0.00191(6)	0.000015(1)	0.0869(6)
1239.611629(14)	10	2	A1	9	3	A2	^{P}R(9,3,A2)	6.24(1)	0.0641(5)	0.0582	0.660(24)	0.650(2)			0.0858(18)
1239.778257(20)	10	2	A2	9	3	A1	^{P}R(9,3,A1)	6.37(2)	0.0636(8)	0.0582	0.883(35)	0.650(2)		0.000111(13)	0.0873(27)
1239.952806(17)	9	4	E	8	5	E	^{P}R(8,5,E)	4.29(1)	0.0595(5)	0.0584	0.769(23)	0.655(3)		0.000074(8)	0.0755(20)
1240.251762(11)	13	3	E	12	2	E	^{R}R(12,2,E)	15.56(2)	0.0576(2)	0.0558	0.682(14)	0.621(1)	−0.00192(13)		0.0804(13)
1241.698227(19)	14	5	E	13	4	E	^{R}R(13,4,E)	8.62(2)	0.0541(2)	0.0535		0.602(2)	−0.00111(9)	0.000020(2)	
1242.002920(10)	13	2	E	12	1	E	^{R}R(12,1,E)	16.84(2)	0.0604(1)	0.0565		0.626(1)	−0.00231(12)		
1242.717923(10)	13	1	A2	12	0	A1	^{R}R(12,0,A1)	17.32(3)	0.0608(2)	0.0569		0.628(1)	−0.00238(12)		0.0810(11)
1243.142558(16)	10	3	E	9	4	E	^{P}R(9,4,E)	5.28(1)	0.0609(3)	0.0570		0.638(1)	−0.00328(31)		
1243.369265(19)	15	7	A2	14	6	A1	^{R}R(14,6,A1)	10.97(2)	0.0493(2)	0.0520		0.591(4)	−0.00199(15)		
1244.037172(17)	14	4	A2	13	3	A1	^{R}R(13,3,A1)	9.97(2)	0.0614(2)	0.0544	0.690(10)	0.608(1)	−0.00219(8)	0.000017(2)	0.0733(10)
1244.072667(17)	14	4	A1	13	3	A2	^{R}R(13,3,A2)	9.82(2)	0.0614(2)	0.0544	0.690(10)	0.608(1)	−0.00219(8)	0.000017(2)	0.0733(10)
1246.120908(16)	14	3	E	13	2	E	^{R}R(13,2,E)	10.71(2)	0.0578(2)	0.0552		0.612(1)	−0.00228(17)	0.000020(2)	0.0744(21)
1246.511979(20)	11	2	A2	10	3	A1	^{P}R(10,3,A1)	4.50(1)	0.0667(4)	0.0574		0.641(1)	−0.00363(14)	0.000020(2)	
1246.746775(21)	11	2	A1	10	3	A2	^{P}R(10,3,A2)	4.43(1)	0.0667(4)	0.0574		0.641(1)	−0.00363(14)	0.000020(2)	
1246.767860(20)	10	4	E	9	5	E	^{P}R(9,5,E)	3.99(1)	0.0570(4)	0.0567		0.635(1)	−0.00723(45)		
1248.302906(14)	14	1	A1	13	0	A2	^{R}R(13,0,A2)	11.48(2)	0.0600(2)	0.0560	0.673(20)	0.618(1)	−0.00183(15)		
1249.414534(28)	16	7	A1	15	6	A2	^{R}R(15,6,A2)	3.47(1)	0.0517(3)	0.0516		0.587(5)			
1249.414534(28)	16	7	A2	15	6	A1	^{R}R(15,6,A1)	3.47(1)	0.0517(3)	0.0516		0.587(5)			
1250.54476(15)	10	5	A1	9	6	A2	^{P}R(9,6,A2)	5.53(1)	0.0581(3)	0.0578		0.652(2)		0.000020(2)	
1251.820632(38)	15	3	E	14	2	E	^{R}R(14,2,E)	7.02(3)	0.0562(3)	0.0545		0.604(2)	−0.00321(26)	0.000020(2)	
1253.518248(26)	11	4	E	10	5	E	^{P}R(10,5,E)	3.30(1)	0.0550(5)	0.0555		0.623(1)			
1253.694913(31)	12	2	A2	11	3	A1	^{P}R(11,3,A1)	3.06(1)	0.0619(6)	0.0566		0.633(3)		0.000020(2)	
1253.749377(23)	15	1	A2	14	0	A1	^{R}R(14,0,A1)	7.43(2)	0.0597(3)	0.0552		0.609(1)			

[a] cm/molecule.
[b] cm^{-1} atm^{-1}.
[c] cm^{-1} atm^{-1} K^{-1}.

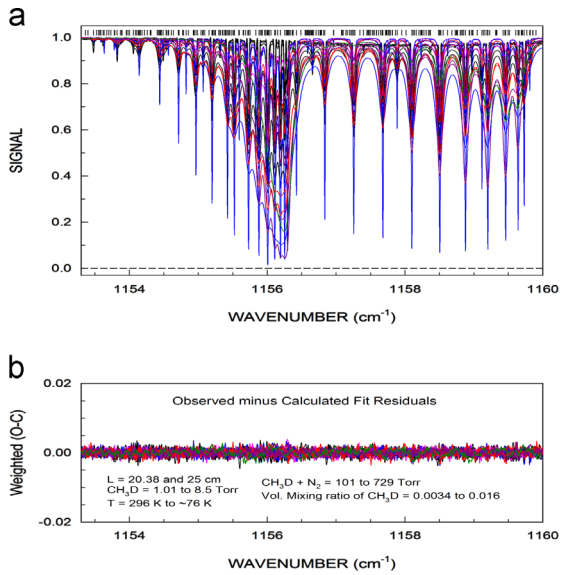

Fig. 4. An example of a multispectrum fit of $^{12}CH_3D$ Triad near 1156 cm^{-1}. 20 spectra are included in this fit. This spectral region shows transitions from the $^{R}Q(J'', K''=0)$ series (band head near 1156.3 cm^{-1}) and transitions from the $^{P}Q(J'', K''=1)$ series (high-wavenumber side), both from the ν_6 band. The observed spectra are plotted in the upper panel (a) and the weighted observed minus calculated differences are shown in the lower panel (b). The horizontal dash line at the bottom of panel (a) represents the 100% absorption level. The short vertical lines seen at the top of the absorption features in (a) correspond to positions of transitions included in the fit. Color codes: room-temperature spectra with the 25 cm cell (black), room-temperature spectra with the 20.38 cm cell (pink); spectra at 240 K (red); spectra at 189 K (blue); spectra at ~135 K (dark pink); spectra at ~76 K (dark green). (For interpretation of the references to color in this figure legend, the reader is referred to the web version of this article.)

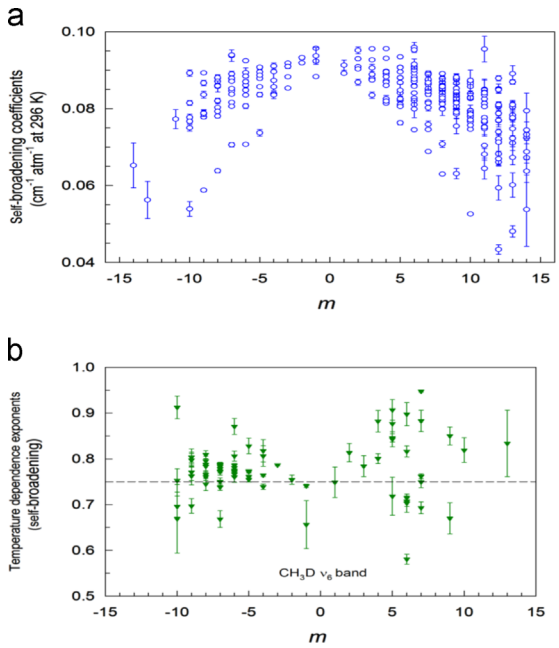

Fig. 5. Lorentz self-broadened line-width coefficients in units of $cm^{-1}atm^{-1}$ in (a) and their temperature dependences (b) plotted against the quantum number index m for transitions in the ν_6 band of CH_3D. The dashed line in panel (b) represents the temperature dependence exponent value 0.75, often used as the default value for transitions where the exponent could not be experimentally determined.

preliminary tests, we retained the dominant contributions with $l_1 \leq 3$ and $l_2 \leq 2$: $V^{00\ eda}_{123}$, $V^{00\ da}_{101}$, $V^{00\ da}_{121}$, $V^{00\ ia}_{224}$, $V^{00\ ia}_{202}$, $V^{00\ ea}_{303}$, $V^{00\ ea}_{323}$, and $V^{00\ ea}_{325}$.The molecular parameters for the accounted long-range and atom–atom interactions are gathered in Tables 3 and 4, respectively.

To get the isotropic potential governing the relative-motion trajectories we fitted the $V^0_{000}(r)$ curve by a standard 12:6 Lennard–Jones function and slightly optimized the σ-parameter (defined below) value to improve the agreement with measurements for high J values (a procedure of "trials" similar to that previously employed for the CH_3Cl-H_2 system [66]). The Lennard–Jones parameters obtained are $\varepsilon=83.50$ K and $\sigma=3.838$ Å. The molecular rotational constants used in the calculations are $A_0=5.2502$ cm^{-1}, $B_0=3.8800$ cm^{-1} [67] for the ground state of the active molecule and $A=5.28744$ cm^{-1}, $B=3.87553$ cm^{-1} [28] for the vibrationally excited ν_6 state whereas $B_0=1.989622$ cm^{-1} [68] for the linear perturbing molecule. At the temperatures of interest only the vibrational ground state has significant rotational populations.

5. Spectroscopic results and comparisons with theoretical results

In Fig. 2 we have plotted examples of pure-gas (panel (a)) and lean CH_3D-N_2-mixture (panel (b)) spectra recorded at 189 K and covering the Triad region between 1070 and 1540 cm^{-1}. Examples of multispectrum-fitted intervals are presented in Figs. 3 and 4. The top panel of Fig. 3 shows P-branch transitions with $J''=16$ and $K=0$–12 relevant to the ν_6 band. The top panel of Fig. 4 presents transitions from the $^{R}Q(J'', K''=0)$ series (band head near 1156.3 cm^{-1}) as well as transitions from the $^{P}Q(J'', K''=1)$ series (high-wavenumber side). In the bottom panels of both Figs. 3 and 4 we have plotted the weighted fit residuals (observed minus calculated) for all spectra included in the multispectrum fits.

The measured zero-pressure line position (ν) in cm^{-1}, N_2-broadened line-width coefficient, b^0_L (N_2) in cm^{-1} atm^{-1} at 296 K, N_2-pressure-shift coefficient δ° (N_2) in cm^{-1} atm^{-1} at 296 K, and their temperature dependences n_1 (unitless) and δ' (cm^{-1} atm^{-1} K^{-1}) are listed in Table 5. Despite the relatively low pressures of CH_3D in our gas samples, in many cases it was necessary to adjust the self-broadened line-width coefficients and their temperature dependence exponents to fit all spectra satisfactorily, and the resulting values determined from the fits are listed in Table 5 and plotted in Fig. 5.

As stated earlier, it was not possible to unambiguously determine from our spectra the CH_3D self-shift coefficients or temperature dependences, and they are not reported here.

In Fig. 5a we have plotted the room-temperature self-broadening coefficients in units of cm^{-1} atm^{-1} against the quantum index m for transitions in the ν_6 band of CH_3D. Here, $m=J''+1$ for the R-branch, $m=J''$ for the Q-branch, and $m=-J''$ for the P-branch transitions, where J is the rotational quantum number of the lower state. The points on Fig. 5 and

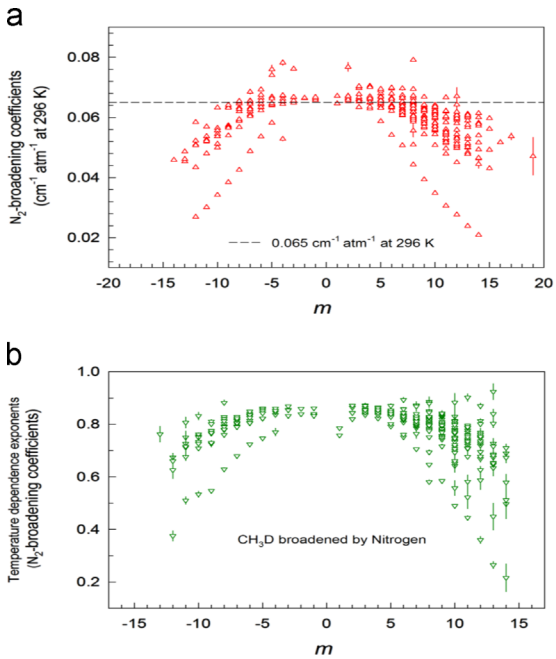

Fig. 6. Lorentz N_2-broadened line-width coefficients (a) and their temperature dependences (b) plotted against the rotational quantum index m for transitions in the ν_6 band of CH_3D. The dashed line represents the mean N_2-broadened line-width coefficient for transitions of this band. N_2-shift coefficients (a) and their temperature dependences (b) plotted against the rotational quantum index m for transitions in the ν_6 band of CH_3D. The dashed line in panel (a) represents the zero-shift value. The error bars represent one standard deviation. In this analysis the temperature dependence for N_2-pressure-shift coefficients were measured where appropriate. For unmeasured transitions their values were fixed to a default value of $+0.00002\ cm^{-1}\ atm^{-1}\ K^{-1}$. This assumption introduced no noticeable residuals in the least squares fits.

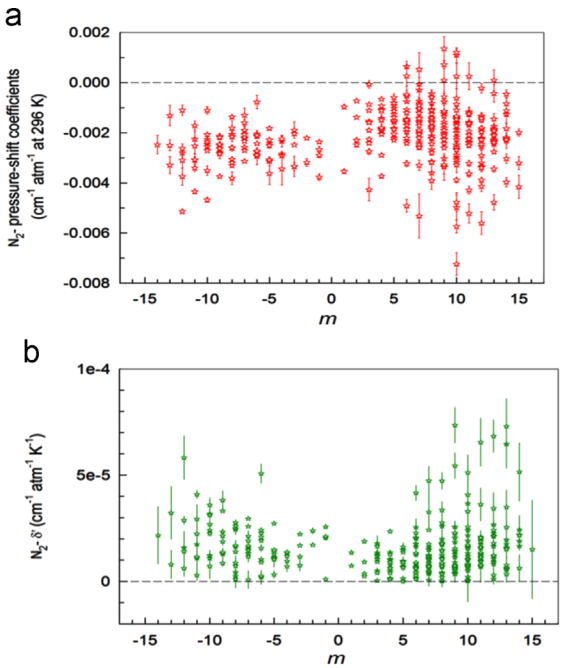

Fig. 7. N_2-shift coefficients (a) and their temperature dependences (b) plotted against the quantum index m for transitions in the ν_6 band of CH_3D. The dashed line in panel (a) represents the zero-pressure value. The error bars represent one standard deviation. In this analysis the temperature dependence for N_2-pressure-shift coefficients were measured where appropriate. For unmeasured transitions their values were fixed to a default value of $+0.00002\ cm^{-1}\ atm^{-1}\ K^{-1}$. This assumption introduced no noticeable residuals in the least squares fits.

6 with smaller broadening coefficients correspond to $^{P}P(J'',K'')$ and $^{R}R(J'',K'')$ transitions for which $J''=K''$. To aid in theoretical calculations we are providing the expression for these smaller broadening coefficients as a function:

$$b_L^0(\text{self}) = 7\times10^{-6}m^3 - 0.0004m^2 - 0.0005m + 0.0899. \quad (6)$$

The measured self- temperature dependence exponents are plotted in panel (b) of the same figure.

Similarly, in Fig. 6 we present our experimental results for N_2-broadening coefficients in panel (a) and their temperature-dependence exponents panel (b), both plotted against values of m. As we did for Fig. 5, the expression for the smaller $J''=K''$ broadening coefficients is:

$$b_L^0(N_2) = -1\times10^{-8}m^5 + 1\times10^{-6}m^4 + 1\times10^{-6}m^3 - 0.0004m^2 + 4\times10^{-5}m + 0.0678. \quad (7)$$

Both the N_2- and self-broadening coefficients from the present study are in very good agreement with the room-temperature values determined in Ref. [35]. The N_2- and self- broadening temperature dependence exponents determined here for the $^{12}CH_3D$ ν_6 band were found to be of similar magnitude as the temperature dependences experimentally determined for air- and self-broadened $^{12}CH_4$ and $^{13}CH_4$ transitions in the same spectral region over a smaller temperature range [50–53]. We also note that for the four ν_6 transitions also measured by Varanasi and Chudamani [43] over the range from 123 K to 295 K, our N_2- and self-widths and temperature dependence exponents (measured over a larger temperature range) are in reasonable agreement within the absolute uncertainties of the two studies.

Our measured N_2-shift coefficients that are included in Table 5 and plotted in Fig. 7 lie between -0.007 and $0.002\ cm^{-1}\ atm^{-1}$ at 296 K. The retrieved temperature-dependences for N_2- pressure-shift coefficients have also been plotted as a function of m in Fig. 7(b)). It is difficult to recognize a trend in the values for the retrieved N_2-shift coefficients due to the relatively small number of data points. However, we do note that the N_2-shift coefficients from the present study are very close to the room-temperature values determined in Ref. [35], and the N_2-shift temperature dependence coefficients determined here for the $^{12}CH_3D$ ν_6 band are quite similar in magnitude to temperature dependences experimentally determined for air-broadened $^{12}CH_4$ shifts in the ν_4 band [50].

Fig. 8 presents overlaid experimental and calculated J-dependences of room-temperature CH_3D-N_2 broadening coefficients at various K values for two sub-branches ^{R}R and ^{P}R in the ν_6 band. The agreement between theoretical and retrieved N_2-broadening coefficients is best for K values below 7. Unfortunately the J-range of our retrieved line parameters is much smaller than that of theoretical

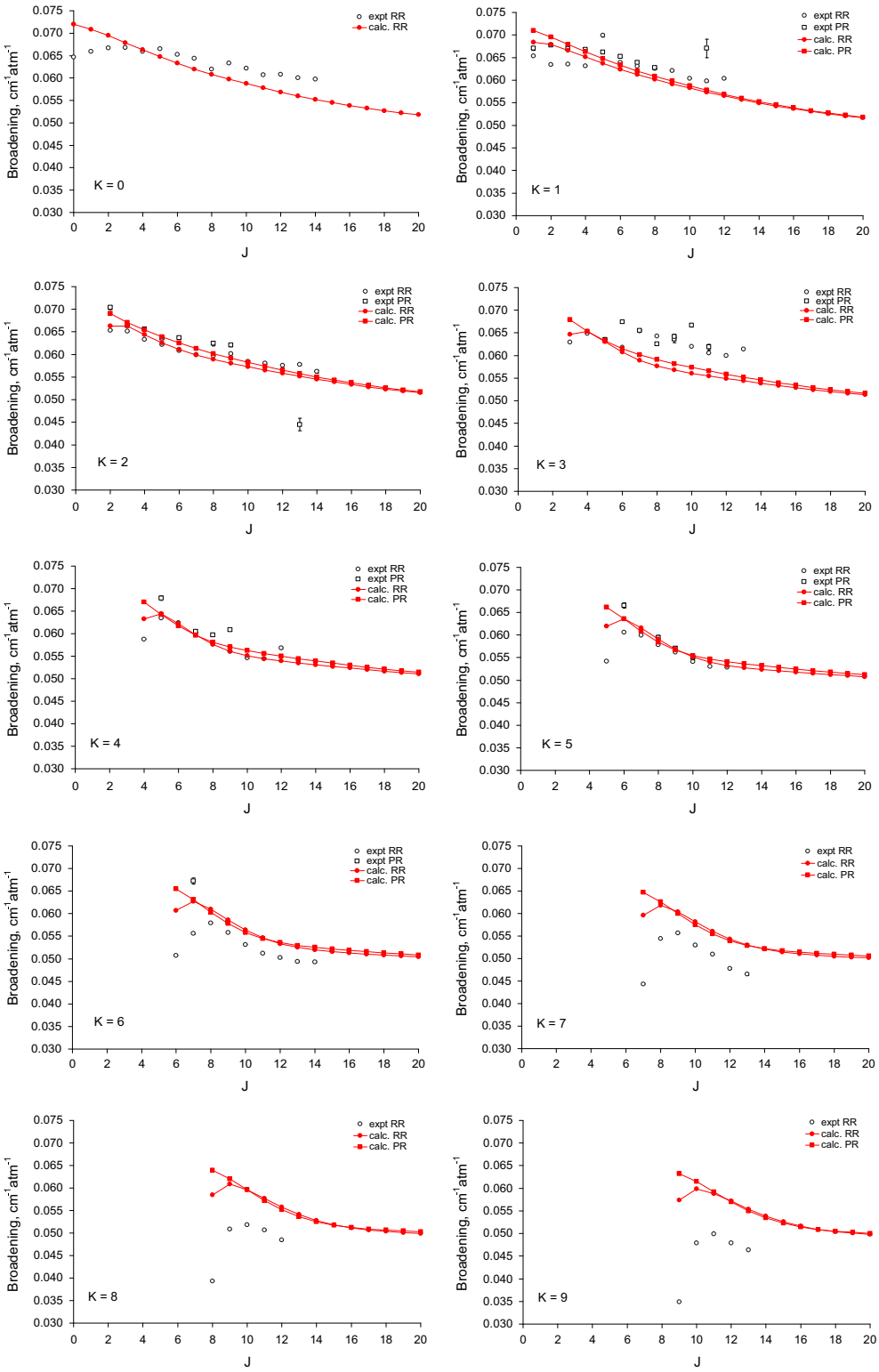

Fig. 8. Comparison of experimental and calculated *J*-dependences of room-temperature CH_3D-N_2 broadened line-width coefficients at various *K* values for the two sub-branches ^{R}R and ^{P}R in the ν_6 band.

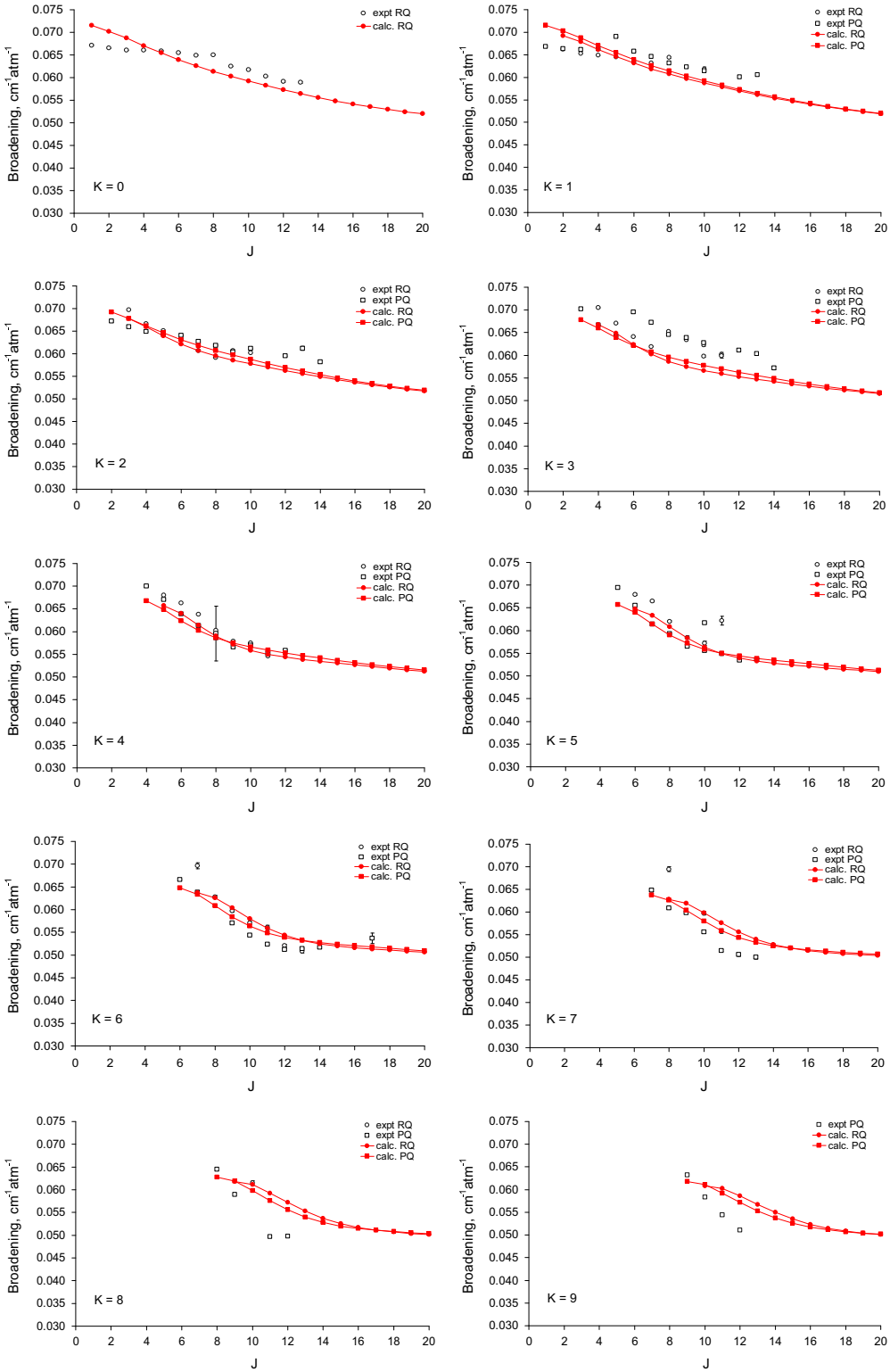

Fig. 9. Comparison of experimental and calculated *J*-dependences of room-temperature CH_3D-N_2 broadened line-width coefficients at various *K* values for the two sub-branches ^{R}Q and ^{P}Q in the ν_6 band.

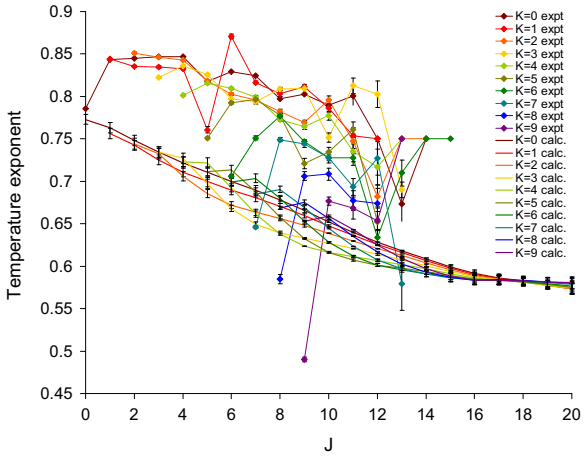

Fig. 10. Theoretical *J*-dependences of the temperature dependence exponents in comparison with the experimental values for ^{R}R-lines.

calculations and we are unable to check the agreement between the two sets of values at high *J* values.

In Fig. 9 we compare retrieved and calculated *J*-dependences of room-temperature CH_3D-N_2 broadening coefficients at various *K* values for the two sub-branches ^{R}Q and ^{P}Q in the ν_6 band. As in the case of the R-branch transitions, the calculations agree better with the experimental values for *K* below 7. Overall, the calculated N_2-broadening coefficients show reasonable agreement with the retrieved N_2-broadening coefficients but for *K* values above 6, they do not reproduce closely the trends in the retrieved line parameters. The general trend in the N_2-broadening coefficients is to remain nearly constant for *K* values below 4, then to drop off rapidly to lower values for larger *K* values. The observed trends in the calculated and observed N_2-broadening coefficients may arise from approximations made in the descriptions of wavefunctions of CH_3D. The calculations performed here are not at the level of accuracy of the tensorial formalism used in the global analysis of positions and intensities of CH_3D.

In order to deduce the temperature dependence exponents for CH_3D-N_2 lines we further calculated the broadening coefficients for two other experimentally probed temperatures: 240 K and 190 K. Lower temperatures were not considered since the thermal motion energy at those temperatures becomes close to the isotropic potential depth (ε=83.50 K) and the semi-classical approaches lose their validity. The temperature exponents *N* were extracted by the usual least-squares method from the relation:

$$\gamma_{if}\ (T) = \gamma_{if}(T_o) \times \left(\frac{T}{T_o}\right)^{-N} \tag{8}$$

where *N* is the n_1 of Eq. (1) and T_o is 296 K, the reference temperature. (In Eq. (8) above, γ=line-broadening coefficient for CH_3D-N_2 and N=n_1 of Eq. (1).)

An example of their comparison with the experimental values is given in Fig. 10 for ^{R}R-branch lines. This figure shows that the theoretical values are generally lower than the corresponding measurements and that for the highest considered *J*, the differences between the calculated curves for various *K* disappear. The discrepancies, as previously, can be attributed to the drawbacks of the semi-classical treatment and the interaction potential model. Theoretical values for line-broadening coefficients at 296 K and the associated temperature exponents are included in Table 5.

A Voigt line shape including line mixing via full relaxation matrix formulation was used to fit the data and improve the residuals. The pressure and path-length products for our spectra listed in Table 1 were not large enough in order to distinguish easily speed-dependence and line-mixing effects. Hence, the speed-dependence parameters could not be retrieved in our analysis, and it was possible to measure the off-diagonal relaxation matrix elements (ORME) for N_2-broadening only for the sets of transitions included in Table 6. We have been able to retrieve the temperature dependences for the relaxation matrix elements for only a few CH_3D+N_2 cases, using an exponential temperature dependence law similar to that used for broadening coefficients. The results for these parameters are also included in Table 6.

6. Conclusions

This study reports experimental measurements of N_2-broadening and pressure-shift coefficients as a function of temperature in the ν_6 band of CH_3D. For the line-broadening case, semi-classical calculations are provided as well. A set of 23 spectra have been analysed to provide accurate values for zero-pressure line-center positions, self- and N_2-broadening coefficients and self- and N_2-pressure-shift coefficients for 400 transitions and their temperature dependences. We have identified several interesting patterns in the measured N_2-broadening coefficients. In addition we have retrieved line mixing (off-diagonal relaxation matrix elements) and where possible, their temperature dependence exponents.

The agreement between the retrieved N_2-broadening coefficients and the semi-classical theoretical results is good, except for higher *K* values where the theoretical results seem to be overestimated. Unfortunately, the experimental N_2-pressure shift coefficients are generally

Table 6
Zero – pressure line positions, width and shift parameters and the off-diagonal relaxation matrix-element coefficients, W_{ij}, determined for pairs of sub-band transitions in the ν_6 band of $^{12}CH_3D$. The fixed parameters are reported with a "(F)" label attached to them.

Position[a]	$b_L^0(N_2)$[b]	$n\ b_L^0(N_2)$	$\delta^0(N_2)$[b]	$\delta'(N_2)$[d]	Assignment	W_{ij} (N_2)[b]	T-dep. W_{ij} (N_2)[b]	W_{ij} (N_2)[e]
1085.625324 (8)	0.0633 (2)	0.832 (15)	−0.00110 (15)	+0.000027(2)	^{P}P(10,3,A1)	0.0040 (2)	1.24 (19)	0.0031 (4)
1085.738824 (8)	0.0633 (2)[c]	0.832 (15)[c]	−0.00110 (15)[c]	+0.000027(2)[c]	^{P}P(10,3,A2)			
1094.044024 (5)	0.0642 (2)	0.774 (6)	−0.00214 (11)	+0.000023 (1)	^{P}P(9,3,A2)	0.0048(1)	0.75 (F)	0.0049 (2)
1094.117524 (5)	0.0642 (2)[c]	0.774 (6)[c]	−0.00214 (11)[c]	+0.000023 (1)[c]	^{P}P(9,3,A1)			
1102.423989 (4)	0.0655 (2)	0.779 (8)	−0.00215 97)	+0.000025 (1)	^{P}P(8,3,A1)	0.0045 (2)	0.82(9)	0.0045 (2)
1102.468792 (4)	0.0655 (2)[c]	0.779 (8)[c]	−0.00215 97)[c]	+0.000025 (1)[c]	^{P}P(8,3,A2)			
1110.754522 (7)	0.0645 (1)	0.805 (1)	−0.00218 (4)	+0.000026 (1)	^{P}P(7,3,A2)	0.0034 (1)	0.75 (F)	0.0060 (3)
1110.779654 (12)	0.0655 (2)[c]	0.779 (8)[c]	−0.00215 97)[c]	+0.000025 (1)[c]	^{P}P(7,3,A1)			
1119.025382 (8)	0.0675 (0)	0.814 91)	−0.00210 (3)	+0.000023 (0)	^{P}P(6,3,A2)	0.0048 (1)	0.75 (2)	0.0032 (2)
1119.038034 (12)	0.0675 (0)[c]	0.814 91)[c]	−0.00210 (3)[c]	+0.000023 (0)[c]				
1143.527534 (7)	0.0653 (1)	0.783 (3)	−0.00177 (5)	−0.000004 (0)	^{R}Q(8,3,A2)	0.0031 (1)	0.80 (F)	0.0032 (2)
1143.571634 (8)	0.0653 (1)[c]	0.783 (3)[c]	−0.00177 (5)[c]	−0.000004 (0)[c]	^{R}Q(8,3,A1)			
1154.439430 (16)	0.0590 (2)	0.840 (19)	−0.00186 (12)	−0.000018 (3)	^{R}Q(13,0,A2)			
1154.713917 (12)	0.0591 (1)	0.870 (12)	−0.00135 (11)	+0.000008 (2)	^{R}Q(12,0,A1)	0.00182 (29)	0.75 (F)	
1154.966470 (9)	0.0603 (1)	0.769 (7)	−0.00158 (9)	+0.000013 (2)	^{R}Q(11,0,A2)	0.00385 (27)	0.75 (F)	
1155.199670 (8)	0.0618 (1)	0.776 (4)	−0.00110 (7)	+0.000016 (1)	^{R}Q(10,0,A1)	0.00492 (22)	0.75 (F)	
1155.422423 (7)	0.0625 (1)	0.790 (3)	−0.00116 (7)	+0.000004 (1)	^{R}Q(9,0,A2)	0.00465 (11)	0.75 (F)	
1155.521843 (7)	0.0650 (1)	0.822 (3)	−0.00267 (7)	+0.000018 (1)	^{R}Q(8,0,A1)	0.00561 (15)	0.75 (F)	
1155.728731 (7)	0.0649 (1)	0.824 (2)	−0.00203 (5)	+0.000016 (1)	^{R}Q(7,0,A2)	0.00734 (10)	0.75 (F)	
1155.879355 (7)	0.0655 (1)	0.831 91)	−0.00146 (6)	+0.000013 (1)	^{R}Q(6,0,A1)	0.00628 (8)	0.75 (F)	
1156.004835 (13)	0.0659 91)	0.828 91)	−0.00186 (6)	+0.000007 (1)	^{R}Q(5,0,A2)	0.00625 (6)	0.75 (F)	
1156.108549 (7)	0.0660 (1)	0.855 (1)	−0.00206 (6)	+0.000005 (1)	^{R}Q(4,0,A1)	0.00674 (6)	0.75 (F)	
1156.191028 (7)	0.0660 (1)	0.840 (2)	−0.00190 (7)	−0.000000 (1)	^{R}Q(3,0,A2)	0.00435 (5)	0.75 (F)	
1156.252680 (8)	0.0666 (1)	0.820 (2)	−0.00248 (9)	−0.000009 (1)	^{R}Q(2,0,A1)	0.00279 (5)	0.75 (F)	
1156.293622 (11)	0.0671 (1)	0.758 (2)	−0.00354 (9)	+0.000014 (1)	^{R}Q(1,0,A2)		0.75 (F)	
1162.997143 (10)	0.0639 (1)	0.778 (2)	−0.00124 (4)	+0.000014 (1)	^{P}Q(9,3,A1)	0.0050 (1)	0.80 (F)	
1163.110746 (7)	0.0639 (1)[c]	0.778 (2)[c]	−0.00124 (4)[c]	+0.000014 (1)[c]	^{P}Q(9,3,A2)			
1163.714357 (8)	0.0645 (1)	0.826 (2)	−0.00212 (4)	+0.000026 (1)	^{P}Q(8,3,A2)	0.0048 (1)	1.17 (3)	
1163.787924 (8)	0.0645 (1)[c]	0.826 (2)[c]	−0.00212 (4)[c]	+0.000026 (1)[c]	^{P}Q(8,3,A1)			
1164.381569 (5)	0.0672 (1)	0.828 (2)	−0.00239 (3)	+0.000024 (0)	^{P}Q(7,3,A1)	0.0035 (1)	0.78 (5)	
1164.426483 (5)	0.0672 (1)[c]	0.828 (2)[c]	−0.00239 (3)[c]	+0.000024 (0)[c]	^{P}Q(7,3,A2)			
1164.989362 (4)	0.0696 91)	0.843 (2)	−0.00232 (3)	+0.000025 (0)	^{P}Q(6,3,A2)	0.0063 (1)	1.04 (3)	
1165.014728 (4)	0.0696 91)[c]	0.843 (2)[c]	−0.00232 (3)[c]	+0.000025 (0)[c]	^{P}Q(6,3,A1)			
1203.493135 (28)	0.0571 (2)	0.765 (5)	−0.00263 (5)	+0.000020 (1)	^{Q}P(12,3,A1)	0.0031 (3)	0.75 (F)	
1203.505090 (26)	0.0571 (2)[c]	0.765 (5)[c]	−0.00263 (5)[c]	+0.000020 (1)[c]	^{Q}P(12,3,A2)			
1205.485111 (8)	0.0655 (1)	0.794 (2)	−0.00140 (3)	+0.000002 (0)	^{R}R(7,3,A2)	0.0035 (1)	0.78 (5)	0.0001 (3)
1205.529251 (8)	0.0655 (1)[c]	0.794 (2)[c]	−0.00140 (3)[c]	+0.000002 (0)[c]	^{R}R(7,3,A1)[c]			
1212.252462 (6)	0.0642 (1)	0.809 (2)	−0.00123 (3)	+0.000003 (0)	^{R}R(8,3,A2)	0.0064 91)	1.14 (2)	0.0038 (4)
1212.298834 (8)	0.0642 (1)[c]	0.809 (2)[c]	−0.00123 (3)[c]	+0.000003 (0)[c]	^{R}R(8,3,A1)			
1218.616479 (8)	0.0674 (2)	0.872 (5)	−0.00206 (7)	+0.000012 (1)	^{P}R(6,3,A1)	0.0043 (2)	1.23 (8)	
1218.661262 (9)	0.0674 (2)[c]	0.872 (5)[c]	−0.00206 (7)[c]	+0.000012 (1)[c]	^{P}R(6,3,A2)			
1218.933810 (9)	0.0641 (0)[c]	0.809 (0)[c]	−0.00201 (4)[c]	+0.000002 (0)[c]	^{R}R(9,3,A1)	0.0111(1)	1.09 (0)	
1218.969303 (6)	0.0641 (0)	0.809 (0)	−0.00201 (4)	+0.000002 (0)	^{R}R(9,3,A2)			
1225.452547 (7)	0.0620 (1)	0.752 (6)	−0.00227 (4)	+0.000016 (1)	^{R}R(10,3,A2)	0.0064 (1)	0.94 (7)	0.0018 (5)
1225.488360 (7)	0.0674 (2)[c]	0.872 (5)[c]	−0.00206 (7)[c]	+0.000012 (1)[c]	^{R}R(10,3,A1)			
1225.671923 (9)	0.0656 (1)	0.829 95)	−0.00318 (7)	+0.000018 (1)	^{P}R(7,3,A2)	0.0044 (2)	1.05 (8)	
1225.745502 (9)	0.0656 (1)[c]	0.829 95)[c]	−0.00318 (7)[c]	+0.000018 (1)[c]	^{P}R(7,3,A1)			
1231.811182 (9)	0.0606 (1)	0.813 (9)	−0.00142 (5)	+0.000021 (1)	^{R}R(11,3,A1)	0.0061 (1)	1.12(11)	0.0038 (1)
1231.848733 (9)	0.0606 (1)[c]	0.813 (9)[c]	−0.00142 (5)[c]	+0.000021 (1)[c]	^{R}R(11,3,A2)			
1238.006728 912)	0.0599 (2)	0.803 (16)	−0.00191 (6)	+0.000015 (1)	^{R}R(12,3,A2)	0.0063 (2)	0.90 (19)	
1238.044758 (12)	0.0599 (2)[c]	0.803 (16)[c]	−0.00191 (6)[c]	+0.000015 (1)[c]	^{R}R(12,3,A1)			
1244.037172 (17)	0.0614 (2)	0.690(10)	−0.00220 (8)	−0.000017 (2)	^{R}R(13,3,A1)	0.0060 (3)	0.75 (F)	
1244.072667 (17)	0.0614 (2)[c]	0.690(10)[c]	−0.00220 (8)[c]	−0.000017 (2)[c]	^{R}R(13,3,A2)			

[a] cm^{-1}.
[b] $cm^{-1}\ atm^{-1}$ at 296 K.
[c] These values are constrained to be the same for the two split pairs of transitions.
[d] $cm^{-1}\ atm^{-1}\ K^{-1}$.
[e] Reference [35]: only room temperature off-diagonal relaxation matrix element coefficients were determined.

scattered and we were unable to model them with our theoretical model.

Acknowledgments

The research described in this article was carried out at the College of William and Mary, Jet Propulsion Laboratory (JPL), California Institute of Technology, Connecticut College and NASA Langley Research Center under contracts with the National Aeronautics and Space Administration. A. Predoi-Cross acknowledges the support she received from the National Sciences and Engineering Research Council of Canada and the study leave program at the University of Lethbridge, AB, Canada for providing the opportunity to carry out this investigation. The authors thank NASA's UPPER Atmosphere Research Program for their support of the McMath – Pierce FTS laboratory.

References

[1] EPA. Methane and nitrous oxide emissions from natural sources. Washington, DC, USA: U.S. Environmental Protection Agency; 2010.
[2] U.S. Department of State. Projected greenhouse gas emissions. In: Fourth climate action report to the UN framework convention on climate change. U.S. Department of State, Washington, DC, USA; 2007.
[3] Shakhova N, Semiletov I, Salyuk A, Yusupov V, Kosmach D, Gustafsson O. Extensive methane venting to the atmosphere from sediments of the East Siberian arctic shelf. Science 2010;327:1246–50.
[4] Miller SM, Wofsy SC, Michalak AM, Kort EA, Andrews AE, Biraud SC, Dlugokencky EJ, Eluszkiewicz J, Fischer ML, Janssens-Maenhout G, Miller BR, Miller JB, Montzka SA, Nehrkorn T, Sweeny C. Anthopogenic emissions of methane in the United States. Proc Natl Acad Sci 2013;110(50):20018–22.
[5] Crutzen PJ. Methane's sinks and sources. Nature 1991;350:380–1.
[6] Alperin M, Hoehler T. The ongoing mystery of sea-floor methane. Science 2010;329:288–9.
[7] Irion W, Moyer EJ, Gunson MR, Rinsland CP, Yung YL, Michelsen HA, et al. Heavy ozone enrichments from ATMOS infrared solar spectra. Geophys Res Lett 1996;23:2381–4.
[8] Rinsland CP, Gunson MR, Foster JC, Toth RA, Farmer CB, Zander R. Stratospheric profiles of heavy-water vapor isotopes and CH_3D from analysis of the ATMOS Spacelab 3 infrared solar spectra. J Geophys Res Atmos 1991;96:1057–68.
[9] Lellouch E, Bezard B, Fouchet T, Feuchtgruber H, Encrenaz T, de Graauw T. The deuterium abundance in Jupiter and Saturn from ISO-SWS observations. Astron Astrophys 2001;370:610–22.
[10] Kim JH, Kim SJ, Geballe TR, Kim SS, Brown LR. High-resolution spectroscopy of Saturn at 3 microns: CH_4, CH_3D, C_2H_2, C_2H_6, PH_3, clouds, and haze. Icarus 2006;185:476–86.
[11] Sromovsky LA, Fry PM, Boudon V, Campargue A, Nikitin A. Comparison of line-by-line and band models of near-IR methane absorption applied to outer planet atmospheres. Icarus 2012;218:1–23.
[12] Burgdorf M, Orton G, van Cleve J, Meadows V, Houck J. Detection of new hydrocarbons in Uranus' atmosphere by infrared spectroscopy. Icarus 2006;184:634–7.
[13] Bezard B, Nixon CA, Kleiner I, Jennings DE. Detection of $^{13}CH_3D$ on Titan. Icarus 2007;191:397–400.
[14] Irwin PGJ, de Bergh C, Courtin R, Bezard B, Teanby NA, Davis GR, et al. The application of new methane line absorption data to Gemini-N/NIFS and KPNO/FTS observations of Uranus' near-infrared spectrum. Icarus 2012;220:369–82.
[15] Mumma MJ, Villanueva GL, Novak RE, Hewagama T, Bonev BP, DiSanti MA, Mandell AM, Smith MD. Strong release of methane on Mars in northern summer 2003. Science 2009;323:1041–5.
[16] Novak RE, Mumma MJ, Villanueva GL. Measurement of the isotopic signatures of water on Mars: implications for studying methane. Planet Space Sci 2011;59:163–8.
[17] Formisano V, Atreya S, Encrenaz T, Ignatiev N, Giuranna M. Detection of methane in the atmosphere of Mars. Science 2004;306:1758–61.
[18] Webster CR, Mahaffy PR. Determining the local abundance of Martian methane and its $^{13}C/^{12}C$ and D/H isotopic ratios for comparison with related gas and soil analysis on the 2011 Mars Science Laboratory (MSL) mission. Planet Space Sci 2011;59:271–83.
[19] Kim SJ, Caldwell J. The abundance of CH_3D in the atmosphere of Titan, derived from 8 μm to 14 μm thermal emission. Icarus 1982;52:473–82.
[20] Coustenis A, Bezard B, Gautier D. Titans atmosphere from Voyager infrared observations 1. The gas composition of Titan's equatorial region. Icarus 1989;80:54–76.
[21] Penteado PF, Griffith CA, Greathouse TK, de Bergh C. Measurements of CH_3D and CH_4 in Titan from infrared spectroscopy. Astrophys J 2005;629:L53–6.
[22] Flasar FM, Achterberg RK, Conrath BJ, Bjoraker GL, Jennings DE, Romani PN, et al. Temperatures, winds, and composition in the Saturnian system. Science 2005;308:1247–51.
[23] Flasar FM, Achterberg RK, Conrath BJ, Gierasch PJ, Kunde VG, Nixon CA, et al. Titan's atmospheric temperatures, winds, and composition. Science 2005;308:975–8.
[24] Kawakita H, Watanabe JI. Fluorescence efficiencies of monodeuteriomethane in comets: toward the determination of the deuterium/hydrogen ratio in methane. Astrophys J 2003;582:534–9.
[25] Kawakita H, Watanabe JI, Furusho R, Fuse T, Boice DC. Nuclear spin temperature and deuterium-to-hydrogen ratio of methane in comet C/2001 Q4 (NEAT). Astrophys J 2005;623:L49–52.
[26] Webster CR, Mahaffy PR. Determining the local abundance of Martian methane and its' $^{13}C/^{12}C$ and D/H isotopic ratios for comparison with related gas and soil analysis on the 2011 Mars Science Laboratory (MSL) mission. Planet Space Sci 2011;2059:271–83.
[27] Pinkley LW, Dangnhu M. Analysis of the ν_6 band of $^{12}CH_3D$ at 8.6 μm. J Mol Spectrosc 1977;68:195–222.
[28] Tarrago G, Delaveau M, Fusina L, Guelachvili G. Absorption of $^{12}CH_3D$ at 6–10 μm: triad ν_3, ν_5, ν_6. J Mol Spectrosc 1987;126:149–58.
[29] Devi VM, Benner CD, Rinsland CP, Smith MAH, Thakur KB. Diode-laser measurements of intensities and halfwidths in the ν_6 band of $^{12}CH_3D$. J Mol Spectrosc 1987;122:182–9.
[30] Tarrago G, Restelli G, Cappellani F. Absolute absorption intensities in the triad ν_3, ν_5, ν_6 of $^{12}CH_3D$ at 6–10 μm. J Mol Spectrosc 1988;129:326–32.
[31] Nikitin A, Champion JP, Tyuterev VG, Brown LR. The high resolution infrared spectrum of CH_3D in the region 900–1700 cm^{-1}. J Mol Spectrosc 1997;184:120–8.
[32] Ulenikov ON, Onopenko GA, Tyabaeva NE, Schroderus J, Alanko S. Study on the rovibrational interactions and A_1/A_2 splittings in the $\nu_3/\nu_5/\nu_6$ triad of CH_3D. J Mol Spectrosc 2000;200:1–15.
[33] Nikitin AV, Champion JP, Tyuterev VG, Brown LR, Mellau G, Lock M. The infrared spectrum of CH_3D between 900 and 3200 cm^{-1}: extended assignment and modeling. J Mol Struct 2000;517–518:1–24.
[34] Devi VM, Benner CD, Smith MAH, Rinsland CP. Measurements of air-broadened width and air-induced shift coefficients and line mixing in the ν_6 band of $^{12}CH_3D$. J Quant Spectrosc Radiat Transf 2001;68:1–41.
[35] Devi VM, Benner CD, Smith MAH, Rinsland CP, Brown LR, Sams RL, et al. Multispectrum analysis of self- and N_2-broadening, shifting and line mixing coefficients in the ν_6 band of $^{12}CH_3D$. J Quant Spectrosc Radiat Transf 2002;72:139–91.
[36] Predoi-Cross A, Hambrook K, Brawley-Tremblay M, Bouanich J-P, Smith MAH. Measurements and theoretical calculations of N_2-broadening and N_2-shift coefficients in the ν_2 band of CH_3D. J Mol Spectrosc 2006;235:35–53.
[37] Blanquet G, Walrand J, Bouanich J-P. Diode-laser measurements of N_2-broadening coefficients in the ν_3 band of CH_3D. J Mol Spectrosc 1995;171:525–32.
[38] Walrand J, Blanquet G, Bouanich J-P. Diode-laser measurements of N_2- and O_2-broadening coefficients in the ν_3 band of CH_3D. Spectroc Acta Part A 1996;52:1037–40.
[39] Devi VM, Benner CD, Smith MAH, Rinsland CP, Brown LR. Multispectrum analysis of self- and nitrogen-broadening, pressure shifting and line mixing in the ν_3 parallel band of $^{12}CH_3D$. J Quant Spectrosc Radiat Transf 2002;73:603–40.
[40] Devi VM, Benner CD, Smith MAH, Rinsland CP, Brown LR. Self- and N_2-broadening, pressure induced shift and line mixing in the ν_5 band of $^{12}CH_3D$ using a multispectrum fitting technique. J Quant Spectrosc Radiat Transf 2002;74:1–41.
[41] Tang Y, Yang SL, Lehmann KK. Measurements of CH_3D line strengths, foreign pressure-broadening, and pressure-shift coefficients at near-IR region using continuous-wave cavity ring-down spectroscopy. J Mol Spectrosc 2013;291:48–56.

[42] Chudamani S, Varanasi P. Measurements on 4.7 μm CH_3D lines broadened by H_2 and N_2 at temperatures relevant to planetary atmospheres. J Quant Spectrosc Radiat Transf 1987;38:179–81.
[43] Varanasi P, Chudamani S. Linewidth measurements in the thermal infrared bands of $^{12}CH_3D$ at planetary atmospheric temperatures. Appl Opt 1989;28:2119–22.
[44] Rothman LS, Gordon IE, Babikov Y, Barbe A, Benner DC, Bernath PF, et al. The HITRAN2012 molecular spectroscopic database. J Quant Spectrosc Radiat Transf 2013;130:4–50.
[45] Sung K, Mantz AW, Brown LR, Smith MAH, Crawford TJ, Devi VM, Benner CD. Cryogenic absorption cells operating inside a Bruker IFS-125HR: First results for $^{13}CH_4$ at 7 μm. J Mol Spectrosc 2010;262: 122–34.
[46] Benner DC, Rinsland CP, Devi VM, Smith MAH, Atkins D. A multi-spectrum nonlinear least squares fitting technique. J Quant Spectrosc Radiat Transf 1995;53:705–21.
[47] Devi VM, Benner D, Smith MAH, Rinsland CP, Brown LR. Measurements of air broadening, pressure shifting and off diagonal relaxation matrix coefficients in the ν_3 band of $^{12}CH_3D$. J Mol Struct 2000;517–518:455–75.
[48] Toth RA. ν_2 band of H_2O: line strengths and transition frequencies. J Opt Soc Am B 1991;8:2236–55.
[49] Rothman LS, Gordon IE, Barbe A, Benner DC, Bernath PF, Birk M, et al. The HITRAN 2008 molecular spectroscopic database. J Quant Spectrosc Radiat Transf 2009;110:533–72.
[50] Smith MAH, Benner DC, Predoi-Cross A, Malathy Devi V. Multi-spectrum analysis of $^{12}CH_4$ in the ν_4 band: I. Air-broadened half widths, pressure-induced shifts, temperature dependences and line mixing. J Quant Spectrosc Radiat Transf 2009;110:639–53.
[51] Smith MAH, Benner DC, Predoi-Cross A, Malathy Devi V. Multi-spectrum analysis of $^{12}CH_4$ in the ν_4 band: II. Self-broadened half widths, pressure-induced shifts, temperature dependences and line mixing. J Quant Spectrosc Radiat Transf 2010;111:1152–66.
[52] Smith MAH, Benner DC, Predoi-Cross A, Malathy Devi V. A multi-spectrum analysis of the ν_4 band of $^{13}CH_4$: widths, shifts, and line mixing coefficients. J Quant Spectrosc Radiat Transf 2011;112: 952–68.
[53] Smith MAH, Benner DC, Predoi-Cross A, Malathy Devi V. Air- and self-broadened half widths, pressure-induced shifts, and line mixing in the ν_2 band of $^{12}CH_4$. J Quant Spectrosc Radiat Transf 2014;133: 217–34.
[54] Ozier L, Ho W, Birnbaum G. Pure rotational spectrum and electric dipole moment of CH_3D. J Chem Phys 1969;51:4873–80.
[55] Robert D, Bonamy J. Short-range force effects in semi-classical molecular line broadening calculations. J Phys (Paris) 1979;40: 923–43.
[56] Ma Q, Tipping RH, Boulet C. Modification of the Robert–Bonamy formalism in calculating Lorentzian half-widths and shifts. J Quant Spectrosc Radiat Transf 2007;103:588–96.
[57] Buldyreva J, Bonamy J, Robert D. Semiclassical calculations with exact trajectory for N_2 rovibrational Raman linewidths at temperatures below 300 K. J Quant Spectrosc Radiat Transf 1999;62:321–43.
[58] Buldyreva J, Nguyen L. Extension of the exact trajectory model to the case of asymmetric tops and its application to infrared nitrogen-broadened linewidths of ethylene. Phys Rev A 2008;77 042720-041.
[59] Buldyreva J, Guinet M, Eliet S, Hindle F, Mouret G, Bocquet R, Cuisset A. Theoretical and experimental studies of CH_3X-Y_2 rotational line shapes for atmospheric spectra modelling: application to room-temperature CH_3Cl-O_2. Phys Chem Chem Phys 2011;13:20326–34.
[60] Nikitin AV, Rey M, Tyuterev VG. Rotational and vibrational energy levels of methane calculated from a new potential energy surface. Chem Phys Lett 2011;501:179–86.
[61] Bouanich J-P, Blanquet G, Populaire J-P, Walrand J. Nitrogen broadening of acetylene lines in the ν_5 band at low temperature. J Mol Spectrosc 1998;190:7–14.
[62] Jacquiez K, Blanquet G, Walrand J, Bouanich J-P. Diode-laser measurements of O_2-broadening coefficients in the ν_3 band of CH_3D. J Mol Spectrosc 1996;171:386–9.
[63] Gray CG, Gubbins KE. Theory of molecular fluids.Fundamentals, vol. 1. Oxford: Clarendon press; 1984.
[64] Bouanich J-P, Blanquet G, Walrand J. Theoretical O_2- and N_2-broadening coefficients of CH_3Cl spectral lines. J Mol Spectrosc 1993;161:416–26.
[65] Buldyreva J, Bonamy J, Weikl MC, Beyrau F, Seeger T, Leipertz A, et al. Linewidth modelling of C_2H_2-N_2 mixtures tested by rotational CARS measurements. J Raman Spectrosc 2006;37:647–54.
[66] Buldyreva J, Rohart F. Experimental and theoretical studies of room-temperature sub-millimetre $CH_3^{35}Cl$ line shapes broadened by H_2. Mol Phys 2012;110:2043–53.
[67] Predoi-Cross A, Hambrook K, Brawley-Tremblay M, Bouanich J-P, Devi VM, Benner DC, et al. Measurements and theoretical calculations of self-broadening and self-shift coefficients in the ν_2 band of CH_3D. J Mol Spectrosc 2005;234:53–74.
[68] Reuter D, Jennings DE, Brault JW. The $\nu=1\leftarrow0$ quadrupole spectrum of N_2. J Mol Spectrosc 1986;115:294–304.